Icarus 293 (2017) 8–26

Contents lists available at ScienceDirect

Icarus

journal homepage: www.elsevier.com/locate/icarus

Long-lived volcanism within Argyre basin, Mars

Jean-Pierre Williams[a,*], James M. Dohm[b], Richard J. Soare[c], Jessica Flahaut[d], Rosaly M.C. Lopes[e], Asmin V. Pathare[f], Alberto G. Fairén[g,h], Dirk Schulze-Makuch[i,j], Debra L. Buczkowski[k]

[a] Department of Earth, Planetary, and Space Sciences, University of California, Los Angeles, CA 90095, USA
[b] Earth-Life Science Institute, Tokyo Institute of Technology, Tokyo, Japan
[c] Department of Geography, Dawson College, Montreal, H3Z 1A4, Canada
[d] IRAP, University of Tolouse, Tolouse, France
[e] Jet Propulsion Laboratory, California Institute of Technology, Pasadena, CA 91109, USA
[f] Planetary Science Institute, Tucson, AZ 85719, USA
[g] Department of Planetology and Habitability, Centro de Astrobiología (CSIC-INTA), Madrid, Spain
[h] Department of Astronomy, Cornell University, Ithaca, New York, USA
[i] Center of Astronomy and Astrophysics, Technical University Berlin, Berlin, Germany
[j] School of the Environment, Washington State University, Pullman, Washington, USA
[k] Applied Physics Laboratory, Johns Hopkins University, Laurel MD 20723, USA

ARTICLE INFO

Article history:
Received 7 November 2016
Revised 26 March 2017
Accepted 4 April 2017
Available online 5 April 2017

ABSTRACT

The Argyre basin, one of the largest impact structures on Mars with a diameter >1200 km, formed in the Early Noachian ~3.93 Ga. The basin has collected volatiles and other material through time, and experienced partial infilling with water evident from stratigraphic sequences, crater statistics, topography, and geomorphology. Although volcanism has not been previously associated with the Argyre basin, our study of the northwest portion of the basin floor has revealed landforms suggesting volcanic and tectonic activity occurred including Argyre Mons, a ~50 km wide volcanic-structure formed ~3 Ga. Giant polygons with a similar surface age are also identified on terrain adjacent to the base of Argyre Mons, indicating the structure may have formed in a water-rich environment. In addition to Argyre Mons, cones, vents, mounds, dikes, and cavi or hollows, many of which are associated with extensional tectonics, are observed in the region. Multiple features appear to disrupt icy (and largely uncratered) terrain indicating a relatively young, Late Amazonian, formation age for at least some of the volcanic and tectonic features. The discovery of Argyre Mons, along with additional endogenic modification of the basin floor, suggests that the region has experienced episodes of volcanism over a protracted period of time. This has implications for habitability as the basin floor has been a region of elevated heat flow coupled with liquid water, water ice, and accumulation of sediments of diverse provenance with ranging geochemistry, along with magma-water interactions.

1. Introduction

The Argyre basin (51°S and 317°E), one of the largest impact structures on Mars with a diameter >1200 km and depth >4 km, is located in the southern highlands southeast of the Tharsis magmatic complex (Scott and Tanaka, 1986; Dohm et al., 2001; Tanaka et al., 2014). The basin has had a complex geologic history since its formation in the Early Noachian, estimated around 3.93 Ga (Robbins et al., 2013). Stratigraphy, topography, and crater counts indicate that there are at least five major and distinct geological units emplaced within the basin, several interpreted to have resulted from major environmental change and large-scale geologic activity such as the development of Tharsis and the growth of south polar ice sheets (Dohm et al., 2015). The basin has been a sink for volatiles and other materials through time indicated by the geologic mapping investigation of Dohm et al. (2015), including significant influxes of sediments and partial infilling with water. This included the formation of transient lakes, the oldest estimated to approximate the extent of the Mediterranean Sea, about 3.75 million km^3 (Dohm et al., 2015). The basin and its impact-derived structures have been etched by liquid water and water-ice (Parker and Gorsline, 1991; Kargel and Strom, 1992; El Maarry et al., 2013; Soare et al., 2014a,b). Eolian activity has also played a

* Corresponding author.
E-mail address: jpierre@mars.ucla.edu (J.-P. Williams).

http://dx.doi.org/10.1016/j.icarus.2017.04.001
0019-1035/

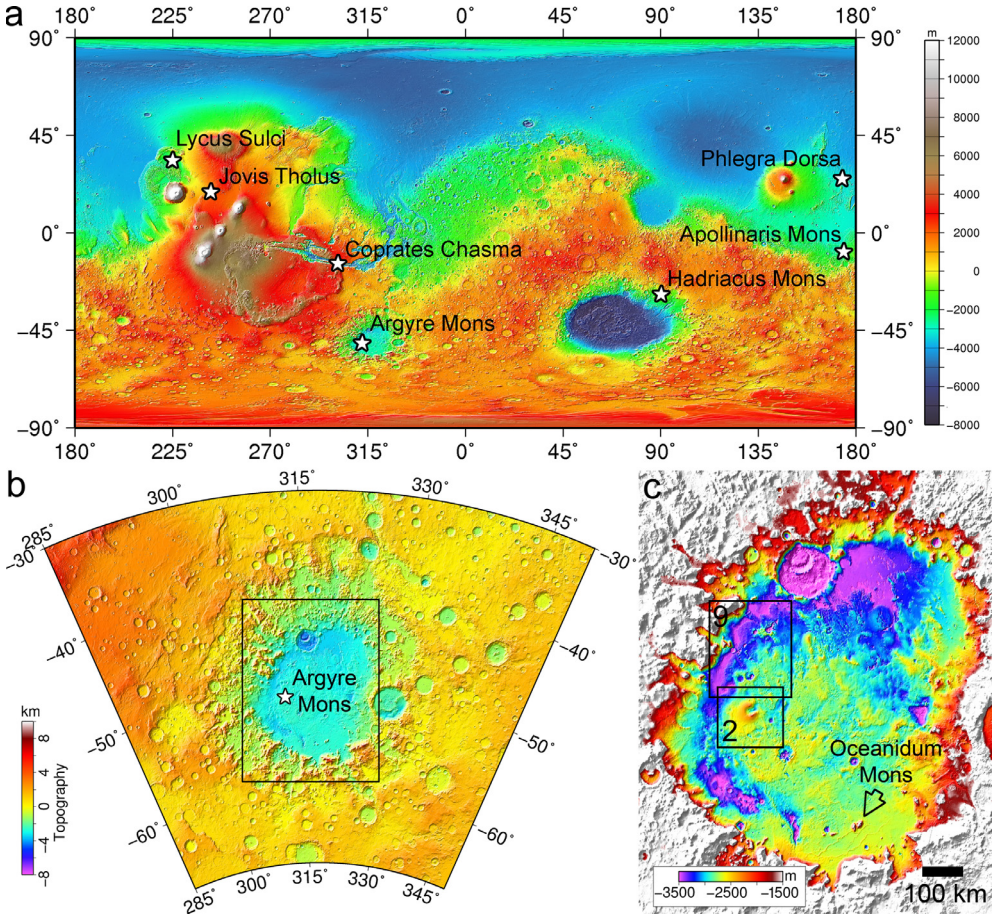

Fig. 1. (a) Global MOLA color shaded relief map with locations of place names discussed in the text labeled. (b) Regional topography map of Argyre Planitia and (c) the Argyre basin floor in conic equidistant projection. Black box in (b) shows location of (c). Black boxes in (b) show locations of Figs. 2 and 9. (For interpretation of the references to colour in this figure legend, the reader is referred to the web version of this article.)

substantial role in contributing to the present-day morphology of the basin floor (Hiesinger and Head, 2002).

Volcanic activity has not been reported to have contributed significantly to the geologic evolution of the Argyre impact structure. Scott and Tanaka (1986) mapped rock materials in the southern portion of the basin as ridged plains using Viking data, with one of their interpretations being a volcanic origin. However, higher-resolution image and topographic data are reportedly more consistent with an esker hypothesis (Kargel and Strom, 1992; Hiesinger and Head, 2002; Banks et al., 2009; Bernhardt et al., 2013). If the ridges are indeed eskers, this would mean that at least part of the basin was occupied by a tens of meters- to possibly kilometers-thick ice sheet with water under hydraulic pressure flowing within or beneath it. Based on stratigraphy and counting all craters $D \geq 3$ km, Dohm et al. (2015) estimated that sedimentation associated with the eskers (the youngest stratigraphic unit) occurred during the Late Hesperian and possibly into the Amazonian.

The discovery of a large (~50 km diameter) feature, Argyre Mons (50.32°S, 311.92°E), on the floor unit of the basin (Williams et al., 2014. 2016; Dohm et al., 2015) represents the first possible large-scale (tens of kilometers wide) volcanic structure presently identified in Argyre Planitia. The feature name, Argyre Mons, was officially approved by the International Astronomical Union (IAU) Working Group for Planetary System Nomenclature shortly after its discovery (Williams et al., 2014) and is described further in this paper. The edifice rises 0.5–1 km above the surrounding basin floor. Aside from a few small ridges at the southeastern margin of the basin (such as Oceanidum Mons), Argyre Mons is the tallest feature on the basin floor (Fig. 1). The size and shape of this edifice is similar to some shield volcanoes on Mars. Additional analysis of image and topography data of the northwestern portion of the basin floor in the vicinity of Argye Mons reveals a suite of spatially-associated features consistent with magma-ice interaction. This includes cavi or hollows, and maar-like craters, many of which are associated with extensional tectonics, and aqueous erosion indicative of melting and/or dewatering of the basin deposits.

In this paper, we describe Argyre Mons and other volcanic and tectonic features in the northwest portion of the basin floor. This endogenic activity represents a previously unrecognized aspect of the geologic history of the basin.

2. Data and methods

Our study of the northwest portion of Agyre Planitia included analysis of image, topography, and spectral data from multiple missions. Image data included individual ConTeXt Camera (CTX) images (5–6 m/pixel) (Malin et al., 2007) from the Mars Reconnaissance Orbiter (MRO), the Mars Odyssey Thermal Emission Imaging System (THEMIS) daytime near-infrared 100 m/pixel resolution mosaic (Christensen et al., 2004), and Mars Express High Resolution Stereo Camera (HSRC) images (nominally 10–20 m/pixel) (Jaumann et al., 2007). Images from MRO's High Resolution Imaging Science Experiment (HiRISE) (McEwen et al., 2007) of the basin floor are limited and therefore our study primarily focused on analysis of CTX images, however, HiRISE images of morphologic analogs within other regions of Mars were used when available. Topographic information was derived from the 128 pixel/degree grid-

ded Mars Orbiter Laser Altimeter (MOLA) (Zuber et al., 1992; Smith et al., 2001, 2003) data. All figures are displayed with north up.

Crater counts were conducted using the Cratertools plug-in for ESRI ArcGIS (Kneissl et al., 2011) to measure crater diameters. Absolute model ages were calculated using Craterstats (Michael and Neukum, 2010) assuming the crater chronology system of Hartmann (2005).

Available Visible Near InfraRed (VNIR) hyperspectral and multispectral data from the CRISM instrument were processed and analyzed to constrain terrain composition. CRISM, the spectral-imager onboard Mars Reconnaissance Orbiter, operates in two modes. In targeted mode, CRISM acquired hyperspectral images at 544 different wavelengths (at 6.55 nm/channel) between 0.362 and 3.92 µm, with a spatial resolution of 18–36 m/pixel (Murchie et al., 2007; 2009). Data are acquired by two detectors, the S detector (0–1 µm) and L detector (1–3.92 µm), and delivered as two distinct observations which have to be joined. In passive, fixed pointing mode, CRISM provides multispectral observations at 72 wavelengths over broader scenes; over 70% of the martian surface has been mapped in this mode (e.g., Murchie et al., 2009). CRISM multispectral data are available as pre-processed tiles of joined S and L data, at a resolution of 100–200 m per pixel (Murchie et al., 2007), whereas CRISM hyperspectral data have to be corrected for atmospheric and photometric artifacts and map-projected. These data were processed with CAT (The CRISM Analysis Toolkit) v7.3.1, the software released by the instrument team, as described in Murchie et al. (2009) and Flahaut et al. (2012). Summary parameters, as described in Pelkey et al. (2007) and Viviano-Beck et al. (2014) , were computed to infer the presence of a given mineral, which was then verified by spectral analyses. Two CRISM multispectral tiles cover the study area: tiles t0291 and t0361. Several CRISM observations are only available as visible (S detector) observations, which is not sufficient for mineralogic identification. There are no CRISM targeted observations available as both S and L observations in the study areas but nearby observations were investigated.

3. Evidence for volcanic landforms in Argyre Planitia: observations and inferences

3.1. The morphology of Argyre Mons

Argyre Mons consists of a quasi-circular rim of high-standing material forming a conic structure with a central, caldera-like pit with a diameter ~25 km and flanks extending 10–20 km (Figs. 2 and 3). Steeper sloped, irregular arcuate ridges are preserved at the crest of the north and south flanks; these are possible remnants of a rim structure and form the highest elevations. The topography is more subdued to the west where erosion appears to have removed any expression of a rim here with an incised channel near the crest as a result of possible collapse and/or sapping. The central depression opens eastward creating a horseshoe-shaped crater in planform.

Layering is present within the walls of the central depression of Argyre Mons with terracing, in part, responsible for the layered appearance (Fig. 4a). Terracing could result from differential erosion of layered deposits of varying competency (e.g. friable ash deposits versus more competent lava flows). Alternating layers of darker and lighter material create banding on the walls in places which may result from darker granular material, often forming ripples, interspersed with a fractured, lighter wall rock material (Fig. 4b). A mound near the center of the depression appears to be capped by a similar, fractured, lighter toned material that lies unconformably on more finely and distinctly layered material (Fig. 4c).

A conical vent structure is observed on the north flank of Argyre Mons (Fig. 5), possibly a parasitic cone. This structure, ~5 km in diameter, has a circular central depression ~2 km in diameter

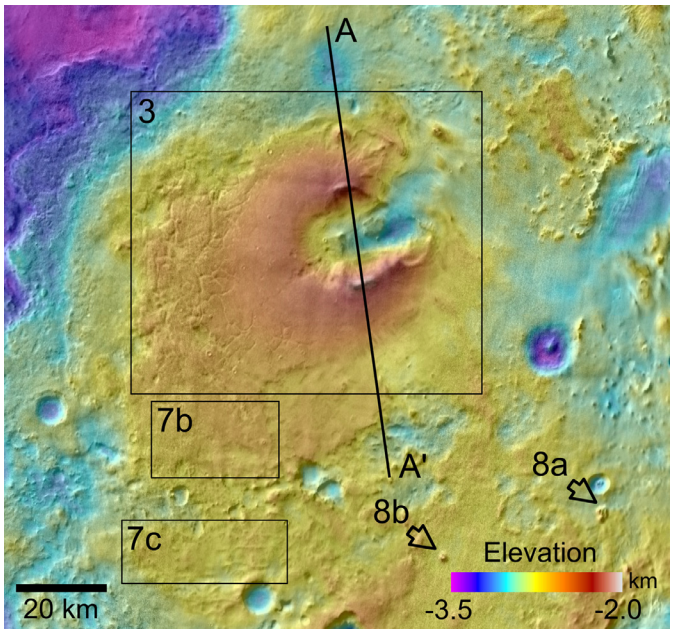

Fig. 2. MOLA color topography of Argyre Mons with the daytime THEMIS IR mosaic used for shading. The black line is the ground track of the topographic profile A – A′ across Argyre Mons in Fig. 20. Boxes show locations of Figs. 3, 7b, and c and arrows show locations of Figs. 8a and b. See Fig. 1 for context. (For interpretation of the references to colour in this figure legend, the reader is referred to the web version of this article.)

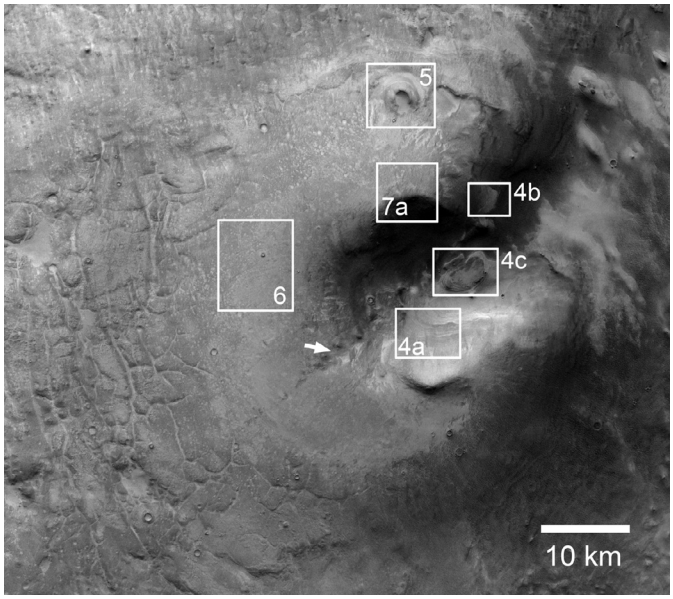

Fig. 3. HRSC nadir channel image hc920_0000 (25 m scaled pixel width) of Argyre Mons and adjacent polygons to the west. White boxes show the locations of Figs. 4–6 and 7a. White arrow highlights channel incised into the southwest wall near the crest. See Fig. 2 for context.

and also horseshoe-shaped similar to Argyre Mons. The flanks are surrounded by a topographic depression or moat except to the south where the northern margin of the flank of Argyre Mons transects the feature. Fine scale layering, most apparent around the rim of the central depression, is fairly concentric and nearly parallel in some instances although in others the layers appear to be folded, indicating that deformation has occurred.

Lobate contacts on the western flank of Argyre Mons are visible where downslope movement of material from the summit area

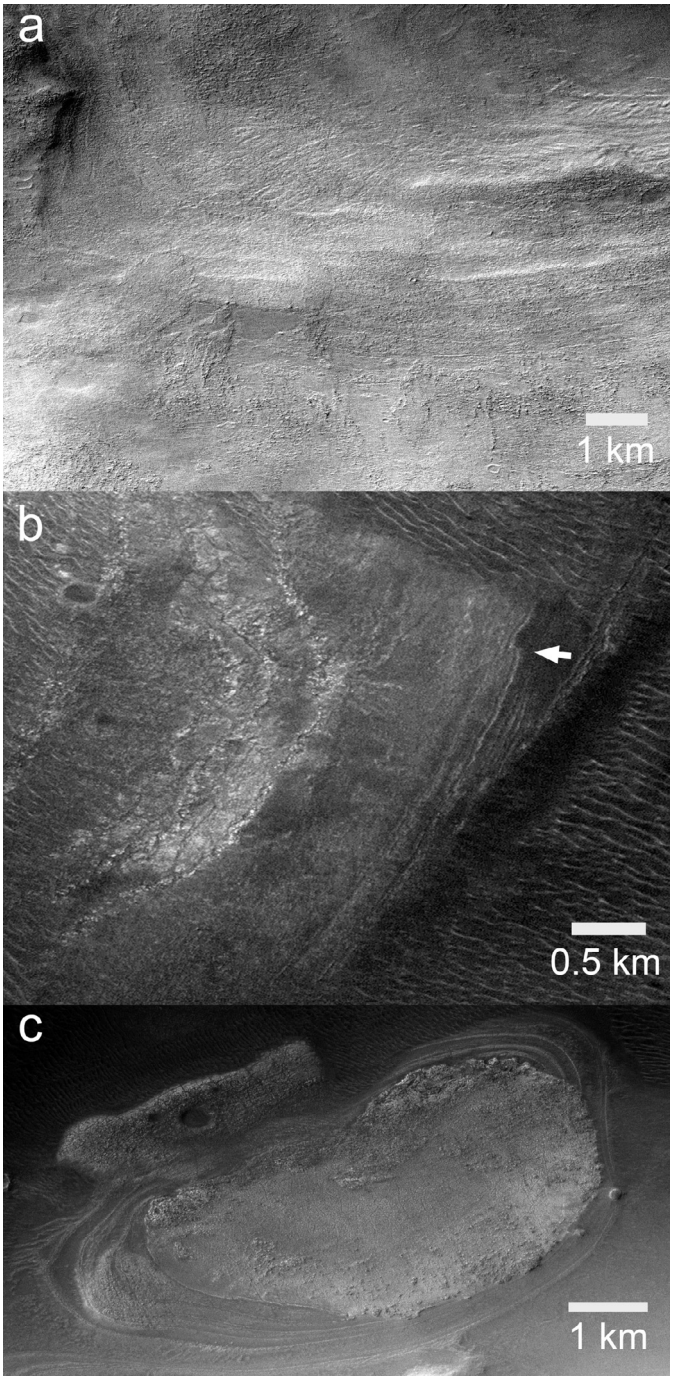

Fig. 4. Portions of CTX image G13_023463_1283_XN_51S047W. (a) Inner wall of south flank displaying terracing. Some terraces are covered by flows of material from mass wasting. (b) Portion of the wall rock of northeastern side of edifice displaying banded appearance. White arrow highlights offset in layers indicating the presence of a fault. (c) A mound of layered material near the center of the depression capped by heavily fractured, lighter-toned material. See Fig. 3 for context.

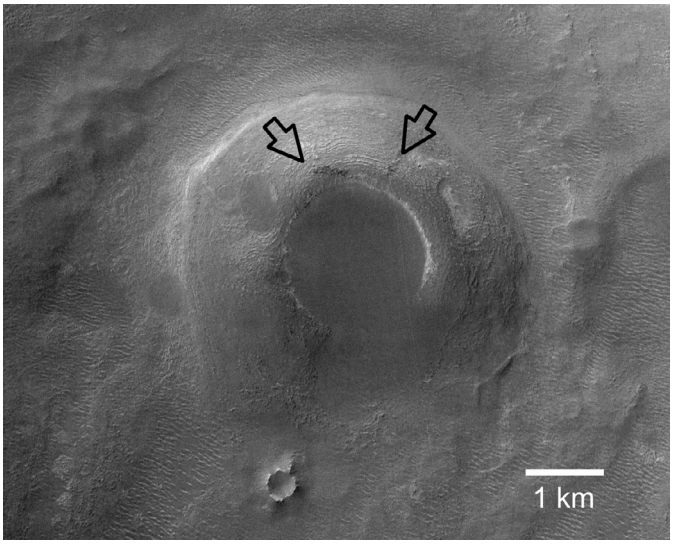

Fig. 5. A ~5 km diameter cone structure on the northern flank of Argyre Mons with distinct, deformed banding (highlighted by arrows) circumferential to the circular summit depression (CTX image: G13_023463_1283_XN_51S047W). See Fig. 3 for context.

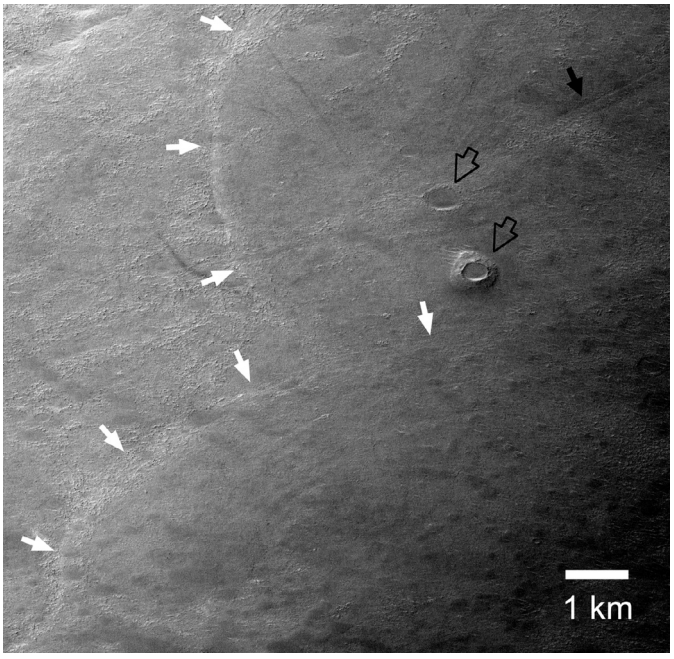

Fig. 6. Overlapping lobate contacts (white arrows) from material that flowed down slope. Material is cross cut by a fault (black arrow). Faint layering is present on the superposed flow. Shallow circular depressions, likely remnant impact craters, and a possible pedestal crater (hollow arrows) indicate the surface has undergone deflation (CTX image: G14_023674_1285_XN_51S048W). See Fig. 3 for context.

terminated. Fig. 6 shows an example of two overlapping flows. Portions of the flows exhibit relatively-smooth surfaces while other parts show textured surfaces as well as faint layering. This could be indicative of surface deflation consistent with the absence of impact craters with fresh morphologies, although there are numerous shallow circular hollows that are likely the remnants of impact craters or the geometric shapes of buried impact craters. A few possible pedestal craters are observed as exemplified in Fig. 6. This feature stands out in contrast to the circular hollows due to its positive relief and well-preserved rim around a central depression. Alternately, this could be a cone structure similar to that observed at the base of the north flank of Argyre Mons though smaller with a diameter ~500 m. Northeast of this feature, a lineament, inferred to be a fault, is also faintly visible cross-cutting the flow material with a lobate margin. Faults are also evident from the offset of layering within Argyre Mons (e.g. Fig. 4b) indicating tectonism in the region. Ridges, some networking and with aligned mounds, such as along the northern flank of the edifice, may have resulted from the intrusion of dikes and the formation of parasitic vent structures, with one intersecting the rim (Fig. 7). Ridges interpreted to be dikes are also observed south of Argyre Mons as aligned mounds,

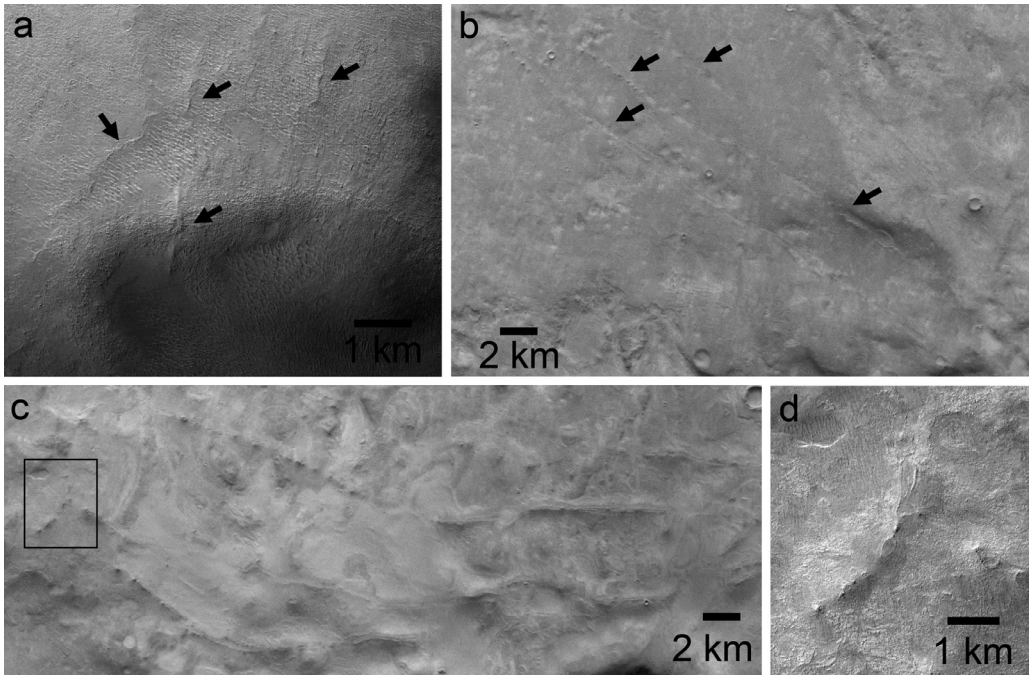

Fig. 7. (a) Ridges (black arrows) on the north rim and flank of Argyre Mons (CTX image: D14_032799_1278_XI_52S049W). See Fig. 3 for context. (b) and (c) Ridges, elongated depressions, and mounds (black arrows) aligned over distances of tens km (HRSC image hc920_0000). See Fig. 2 for context. Box indicates location of (d). (d) Aligned mounds, some with summit depressions (CTX image: D14_032799_1278_XI_52S049W).

ridges, and elongated depressions. Some mounds possess summit depressions and morphologically resemble volcanic cones indicating that fissure eruptions may have occurred along the fractures over distances of tens km.

3.2. Landforms around Argyre Mons

Additional evidence for volcanism and magma/volatile interaction are observed within the vicinity of Argyre Mons including many cones, pits, depressions, mounds, and erosional landforms indicating surface flow and headwall erosion from collapse/sapping. Two smaller structures adjacent to Argyre Mons may also be volcanic in origin (313.65°E, 51.42°S and 312.63°E, 51.60°S). These features are several km in diameter with summit elevations ~150 m above the surrounding basin floor (Fig. 8). The summits of the structures are broad and irregular in shape with the feature in Fig. 8a containing a well-developed circular pit or depression near its center and the other in Fig. 8b containing a relatively sharp-crested arcuate ridge; a possible horseshoe-shaped remnant of a summit crater similar to both Argyre Mons and the vent structure in Fig. 5. Deposits with lobate terminal contacts appear to originate from one of the structures and extend for several km (white arrow in Fig. 8a). These may be flows of volcanic or landslide origin. Volcanic cones of similar size have been identified in Tharsis (Brož and Hauber, 2012), the Nephentes/Amethes region (Brož and Hauber, 2013), Isidis Planitia (Ghent et al., 2012), Elysium Planitia (Noguchi and Kurita, 2015), Melas Chasma (Dohm et al., 2009), and the floor of Coprates Chasma (Hauber et al., 2015).

North of Argyre Mons, numerous elongated and irregular depressions, or cavi, are observed ranging in size from sub-km to tens of km in length (Figs. 9 and 10). In many cases they are aligned with extensional faults and fractures that extend across the region, demonstrating an element of structural control in their formation; some fault segments extend up to ~100 km in length. The cavi appear to be associated with faults and fractures which may have provided conduits for both the migration and withdrawal of volatiles. Many of the cavi contain mounds and ridges that appear to be coherent rock that has remained in place during the formation of the depressions.

A quasi-circular area ~7 km in diameter experienced collapse of the surface to form irregular troughs and ridges with faulting with a preferential southwest-northeast orientation (Fig. 11). Material flowed from the northeast side of the depression forming a deposit downslope that extends ~8 km. The nature of the deposit is unclear and may have resulted from extrusion of lava or fluidized debris-flow from the melting or eruption of water (lahar). Numerous other smaller circular pits, rimmed depressions, and rings of material are observed in the area with some aligned with tectonic features. Given the geologic history of the Argyre basin involving an aqueous and ice-rich environment, it is possible these are remnants of phreatic and phreatomagmatic eruptions in the form of tuff cones, tuff rings, or maars as a result of the explosive interaction of magma with standing water, ground water, or permafrost (Lorenz, 1973, 1986; Sheridan and Wohletz, 1983). The two largest candidate maars we identify in Argyre have diameters ~5 km (Fig. 11d and e) with many smaller candidate maars identified within the region. These craters lack the distinct raised rims and ejecta blankets of impact craters and appear to have fluidized deposits or channels along their flanks.

Direct evidence of lava extrusion is scarce. A candidate lava flow is observed within the floor of a channel (Fig. 12a, b). The source of the flow is unclear but appears to originate near or exterior to the mouth of the channel and flowed east ~10 km into the channel. The flow is obscured outside of the channel by dune forms which bury the deposit, so its total extent is uncertain. At least two flows were emplaced with an underlying deposit observed to extend ~2 km further up the channel beyond an overlying deposit. The two flows form a benched topographic expression on the north contact where the underlying flow is not completely covered by the subsequent flow. Aligned knobs and small cones on the surface may have resulted from the explosive interaction between the surficial lava and near-surface water or ice in the underlying substrate upon which it was deposited to form pseudocraters (or rootless cones).

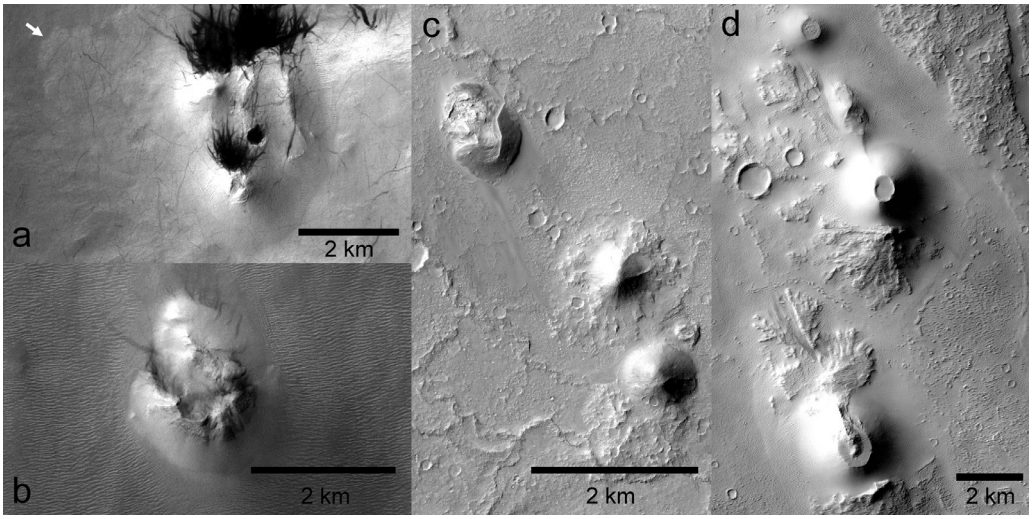

Fig. 8. Examples of potential smaller volcanic structures within the vicinity of Argyre Mons (a) and (b), and morphologically similar features in other regions on Mars associated with volcanism (c) and (d). (a) 313.65°E, 51.42°S (CTX image: G12_023041_1276_XI_52S046W) and (b) 312.63°E, 51.60°S (CTX image: G13_023463_1283_XN_51S047W). See Fig. 2 for context. The diameters of the features are ~1–2 km with elevations of ~150 m making them similar in size to volcanic cones observed in (c) Coprates Chasma at 303.76°E, 14.94°S (HiRISE image ESP_045498_1650, 53.5 cm scaled pixel width) and (d) the pyroclastic cones identified by Brož and Hauber (2012) in Tharsis at 237.04°E, 5.64°N (CTX image: P19_008262_1862_XN_06N123W). The summit of the structure in (a) has a broad (>1 km), irregular shape and topography with a circular pit near the center. Material appearing to originate from or near the structure has been deposited to the northwest where a contact remains visible (white arrow). The summit of the structure in (b) has a central depression that opens to the northwest with a relatively sharp rim on the southwest margin; possibly the remnant of a summit crater. Dark streaks result from the removal of bright dust by winds and dust devils.

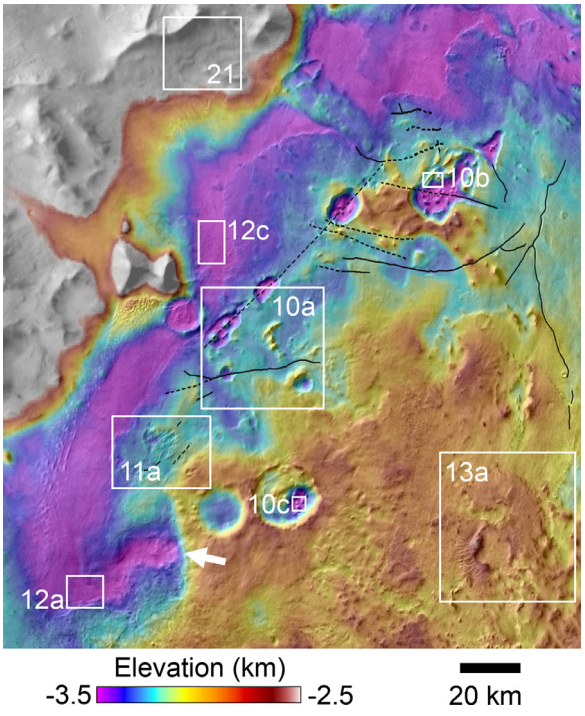

Fig. 9. MOLA topography with the THEMIS IR daytime mosaic used for shading showing the northwest quadrant of the Argyre basin floor north of Argyre Mons. Black solid lines highlight graben and dashed lines where graben are inferred from the alignment of features. White boxes show locations of subframes in Figs. 10a-c, 11a, 12a-c and 21. White arrow highlights location of headwall erosion of canyon. See Fig. 1c for context. (For interpretation of the references to colour in this figure legend, the reader is referred to the web version of this article.)

Possible rootless cones (pseudocraters) elsewhere in the area indicate lava emplacement atop a water or ice-rich surface. Hundreds of circular and elliptical mounts, pitted cones, and rings are observed on deposits on the northwest margin of the Argyre basin floor (Fig. 12c). Rootless cones result from phreatomagmetic explosions as lava mechanically mixes with the water-rich substrate forming cratered cones of ash, scoria, spatter, and lithic material from the underlying substrate (e.g. Thorarinsson, 1953; Thordarson and Höskuldsson, 2008). These features do not overlie volcanic conduits rooted to a magma source, and thus are referred to as rootless cones or pseudocraters. As the activity at a given cone subsides due to volatile depletion or lava supply, explosions will typically initiate elsewhere resulting in groups of tens to hundreds of cones within the flow field with the spatial density indicative of the quantity of water in the substrate at the time of cone formation (Greeley and Fagent, 2001). Rootless cones have been identified elsewhere on Mars (e.g. Lanagan et al., 2001; Fagents et al., 2002; Fagents and Thordarson, 2007; Jaeger et al., 2007; Keszthelyi et al., 2010) and their presence here indicates the basin materials in this region may include a volcanic origin. Figs. 12d and e show other examples of rootless cones we have identified in the volcanic regions of Phlegra Dorsa and Lycus Sulci that are morphologically similar to the cones in Argyre.

Additional structures within the vicinity of Argyre Mons may be remnants of less well-preserved volcanic structures. An example of a candidate structure is shown in Fig. 13 where elevated topography forms arcuate, ~200 m high ridges that appear to outline a possible ~10–20 km wide caldera. Where the caldera rim is preserved to the west and southwest, and to a lesser extent on what remains of an eastern rim, the flanking topography possess a series alternating troughs and ridges spaced fairly uniformly at ~1 km extending radially down slope. Other low-profile, shield-like, volcanoes with large summit-calderas on Mars possess dissected flanks exhibiting similar radial troughs and ridges such as Hadriacus Mons on the northwest rim of Hellas basin and Apollinaris Mons near the dichotomy boundary (Fig. 13). The low slopes, channeled flanks, and smooth caldera floors of these volcanoes indicate construction involving pyroclastics possibly driven by explosive water-magma interaction. The morphology of the prominent channels indicates formation by pyroclastic flows or lahars, with possible modification by subsequent fluvial or ground water sapping processes (e.g. Williams et al., 2007; El Maarry et al., 2012). A canyon, several km wide dissects a plateau of material north of the caldera structure possibly resulting from ground sapping of water and headwall erosion indicating elevated heat flow.

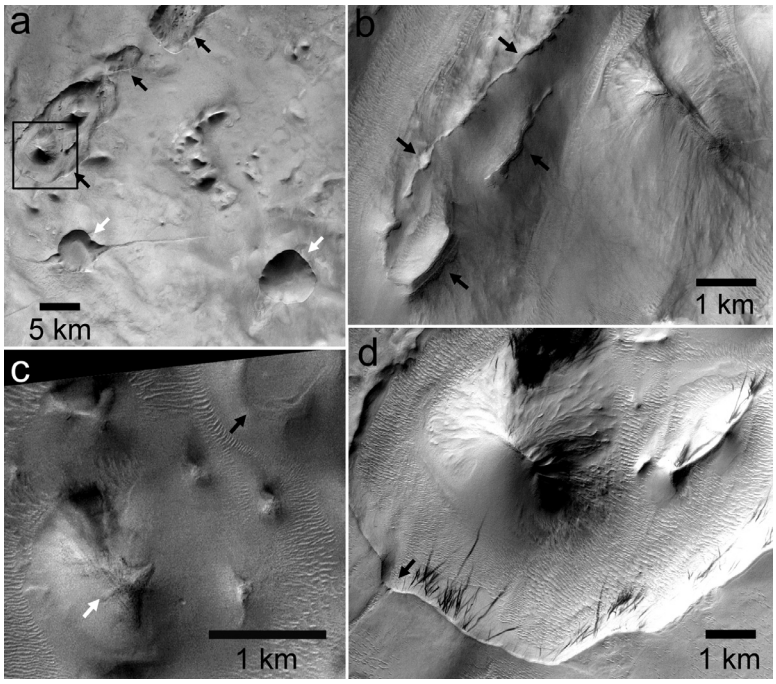

Fig. 10. Evidence for intrusion into ice-rich regolith: (a) Mounds and ridges within cavi (black arrows) and two large (~5 km diameter) candidate maars (white arrows) highlighted in Fig. 11 (HRSC nadir channel image: hc920_0000). Box shows location of (d). (b) Exposed dike- and sill-like features (black arrows) within depression (CTX image: G15_023964_1319_XI_48S046W). (c) Layered pluton-like feature (white arrow) exposed within a ~600 m deep depression and an elliptical, rimmed feature (black arrow), a possible tuff ring or maar formed by magma-water interaction (CTX images: P13_006150_1323_XN_47S048W). (d) km-scale mounds and ridges within a depression possibly resulting from intrusion of near-surface magma. A saddle in the southwest rim with a channel extending down slope indicates the rim was breached by liquid water (black arrow) (CTX image: P13_006150_1323_XN_47S048W). See Fig. 9 for context for (a–c).

3.3. Hydrologic features associated with Argyre Mons

The Argyre basin floor materials have been mapped and interpreted as having a general sedimentary origin by Dohm et al. (2015) deposited under various environmental conditions from a multitude of sources, possibly as far as Tharsis. This includes lake formation as noted above. Additional evidence for past hydrologic activity is observed around Argyre Mons. This includes giant polygons on the west margin of Argyre Mons (Figs. 2 and 3) and a 10–20 km wide amphitheater-headed canyon on the northwest margin of Argyre Mons (Fig. 9). The steep headwall of the canyon with no apparent dissection upstream is diagnostic of erosion by groundwater seepage where the valley head is undermined and propagates upstream (Piere, 1980; Carr and Clow, 1981; Howard et al., 1988; Malin and Carr, 1999; Goldspiel and Squyres, 2000; Grant, 2000). However this formation mechanism has been questioned as some terrestrial amphitheater-headed canyons appear to require surface runoff (Lamb et al., 2006, 2007; Lapotre et al., 2016). Box Canyon, Idaho, for example, appears to have eroded into coherent basalt during a large flooding event (Lamb et al., 2008). However, the estimated amount of water needed to transport the required sediment volumes could have been supplied hydrothermally from volcanic intrusions (Gulick, 1998, 2001).

The giant polygons on the western margin of Argyre Mons (Figs. 2 and 3) are confined to a ~2000 km^2 relatively flat area with an elevation ~−2600 m. The polygon troughs persist to elevations ~150 m below the plateau at the edges indicating the approximate depth of the troughs. The original extent of the polygons is unclear but their restricted elevation implies they formed within a particular stratigraphic horizon within the basin deposits and do not extend up the flank of Argyre Mons. The polygons are highly irregular and angular in shape ranging in size ~1–10 km with rounded, convex, bounding trough walls. Trough widths vary with the larger troughs ~500 m wide. Kilometer-scale polygons have been observed in several locations within the northern lowlands with major occurrences in Acidalia Planitia, Chryse Planitia, Utopia Planitia, and Arcadia Planitia (Oehler, 2014 and references therein). The origin of giant polygons is debated, although the suggested mechanisms for their formation generally involve water, either as ice, water-rich sedimentation, or standing bodies of water (e.g. Pechmann, 1980; McGill, 1986; Hiesinger and Head, 2000; Lane and Christensen, 2000; Cooke et al., 2011; Buczkowski et al., 2012; Oehler and Allen, 2012; Moscardelli et al., 2012). The observation of kilometer-scale polygonal fault systems in terrestrial offshore sedimentary basins in 3-D seismic data provides a terrestrial analog within a marine environment. The geomorphological similarities with giant polygons on Mars have led to the suggestion that the polygons in the northern lowlands on Mars are evidence for the existence of a large body of water or ocean (Moscardelli et al., 2012; Oehler and Allen, 2012; Allen et al., 2013). The onset of polygonal terrain occurring at similar elevations within Utopia basin (Hiesinger and Head, 2000) suggests a correspondence to an equipotential surface consistent with formation being related to a body of liquid water.

3.4. Crater counts

Crater counts were conducted on the flanks of Argyre Mons and the polygons (Fig. 14). Overlapping model ages of ~3 Ga (considering statistical uncertainties noted in Fig. 14b) is obtained for both surfaces using the Hartmann chronology system (Hartmann, 2005) not only indicating that the formation of the polygons and Argyre Mons may have been contemporaneous, but also occurred within the time range of the Late Hesperian-Early Amazonian lake hypothesized by Dohm et al. (2015) as discussed above. Dohm et al. (2015) compiled crater statistics to evaluate the formation and modification ages of the Argyre rock units using craters with $D > 3$ km. The total crater population of the youngest basin unit

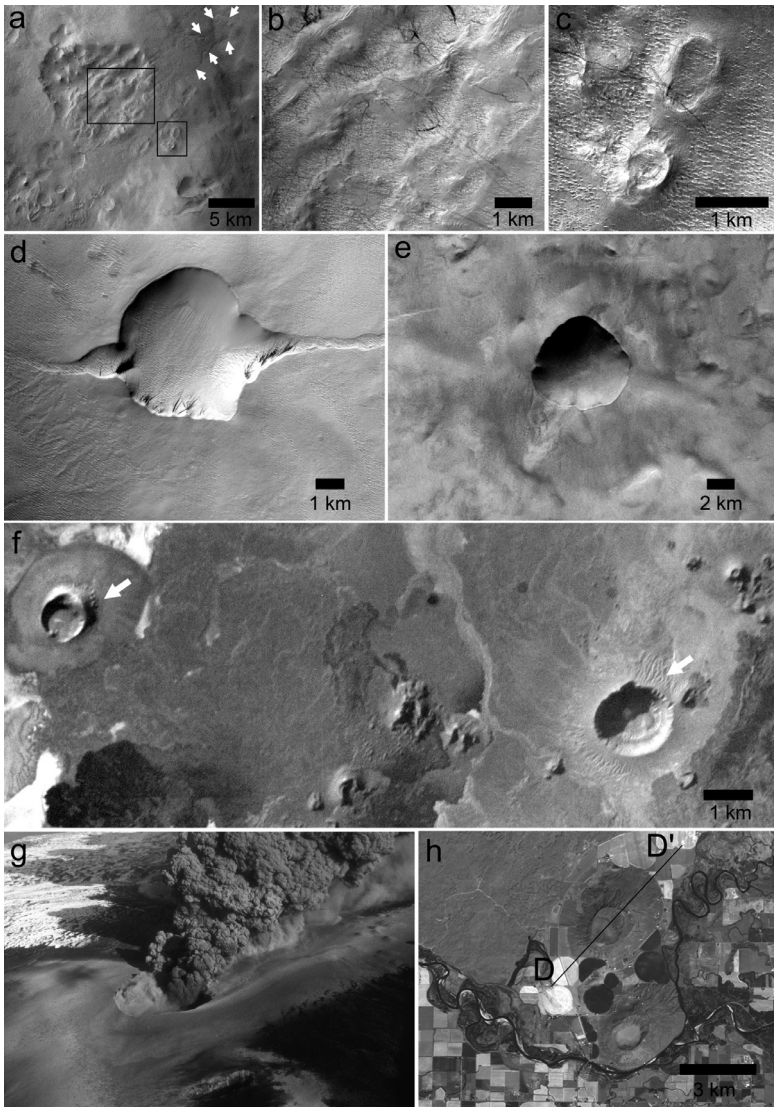

Fig. 11. Landforms indicative of intrusion into ice-rich regolith north of Argyre Mons (a–e) and terrestrial analogs (f–h). (a) A region with southwest-northeast trending faults, depressions, mounds, and ringed pits formed by tectonically controlled intrusion into the near-surface. (CTX images: P19_008510_1329_XI_47S049W, P16_007218_1335_XN_46S049W). Material appears to have flowed northeast down slope from this region (extent of deposit indicated by white arrows). Boxes are locations of (b) and (c). See Fig. 9 for context. (b) Portions of (a) showing elongated irregular depressions or troughs and densely faulted ridges and (c) examples of rings of material possibly resulting from hydrovolcanic eruptions (CTX image: B11_013903_1307_XN_49S048W). (d) A possible maar intersected by a graben. The crater is ~5 km in diameter. Braided deposits are visible on the southwest flank indicating possible extrusion of fluidized material (CTX image: P13_006150_1323_1323_XN_47S048W. (e) Maar-like feature ~5 km in diameter. Lobate deposits are apparent on the southern flank indicating material flowed downslope from the rim (HRSC nadir channel image: hc920_0000). See Fig. 10a for context of (d–e). (f) The Pinacate volcanic field, Sonora, Mexico containing hundreds of cinder cones and eight maars (113.4°W, 31.9°N). The two larger features (white arrows) are the tuff cone of Cerro Colorado (left) and the maar Crater Elegante (right) (portion of image ISS009-E-5944 courtesy of the Earth Science and Remote Sensing Unit, NASA Johnson Space Center, http://eol.jsc.nasa.gov). (g) Aerial photo of the phreatomagmatic eruption in 1977 that formed the East Maar of the Ukinrek Maars in Alaska (156.51°W, 57.83°N) (Kienle et al., 1980; Self et al., 1980; image courtesy of Juergen Kienle). The maar has a diameter of 300 m. The smaller West Maar, which formed first, is visible in the foreground. (h) Menan Buttes tuff cones in southeast Idaho (111.97°W, 43.77°N). Black line: ground track of topographic profile D – D′ in Fig. 20. (Portion of Earth Observing One (EO-1), Middleton et al., 2013, image: EO1A0390292010268110KF_B01).

(HAb4a), which included partly buried, degraded, and pristine impact craters, yielded a model age of ~3.5 Ga. Some of these impact craters could represent older basin units with rims protruding through the younger basin deposits. The pristine craters with distinct rims and ejecta blankets, and lacking visible evidence for resurfacing, produced a model age of ~1.3 Ga. This indicates a period of major resurfacing occurred during the Middle and Late Amazonian epochs that included significant influxes of sediments and partial infilling with water including the formation of lakes. The ~3 Ga model crater-retention age of the flanks of Argyre Mons and the adjacent giant polygons place the formation within this period. Many of the superposed craters are highly degraded with a significant deficit of craters $D \lesssim 300$ m. The presence of several pedestal craters indicates the surfaces have experienced deflation. A severe lack of craters with a fresh appearance at any size implies modification of the surface has persisted to at least the recent past.

3.5. Spectral observations

Most of the flat floor of Argyre is characterized by spectrally bland signatures. This effect could be due to its topography, which is prone to the accumulation of dust (only a few microns would mask potential surface signatures), but also to the low elevation and high latitude of the Argyre basin. Indeed, Argyre basin is particularly affected by high aerosol opacity (longer atmospheric path length) and surface frosts (CO_2 and H_2O), making the investigation

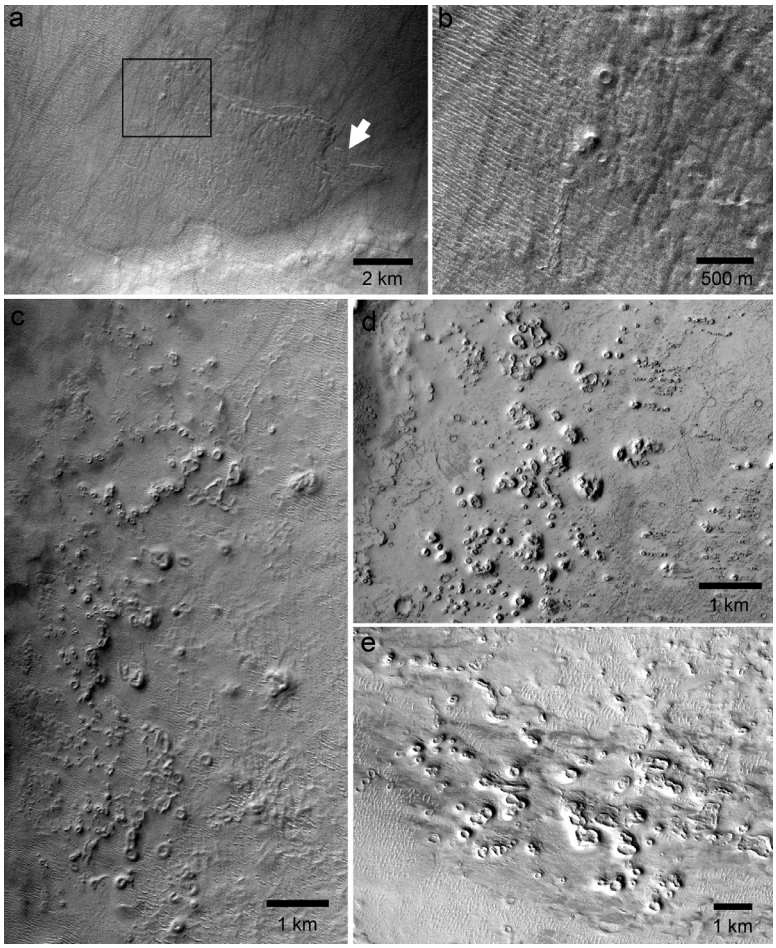

Fig. 12. (a) Extrusive deposit within a channel north of Argyre Mons (CTX image: D14_032799_1278_XI_52S049W). See Fig. 9 for context. White arrow highlights an older deposit and the black box is the location of (b) showing mounds and cones on the surface of the flow. (c) Circular and irregular rings, mounds, and pitted cones. See Fig. 9 for context. These (possible) pseudocraters, result from the emplacement of lava flows on a water-rich substrate and are found in other areas of Mars associated with volcanism such as the Phlegra Dorsa region (d) and the Lycus Sulci region (e) (CTX image: P13_006150_1323_XN_47S048W). (d) Example of possible pseudocraters on lava flows in the Phlegra Dorsa region at 172.46°E, 26.07°N (CTX image B21_017679_2060_XN_26N187W). (e) Example of possible pseudocraters on lava flows in the Lycus Sulci region north of Olympus Mons at 225.10°E, 34.45°N (CTX image B21_017679_2060_XN_26N187W). See Fig. 1a for context.

of its surface composition difficult (e.g., Carter et al., 2013). With this consideration, CRISM spectral signatures indicate the presence of mafics, especially olivine, in the mountains located along the northwest margin of the basin floor (Fig. 15). These spectral signatures could indicate volcanic materials that were deposited from either wind or water from local or more distant provenances (e.g., Tharsis), or emplaced by local volcanism consistent with other lines of evidences discussed in this work. Alternatively, these detections could also represent ejected material from Argyre accumulated in the basin inner rings (e.g., Ody et al., 2013). A spectrally distinct material (possibly olivine or phyllosilicates from the high OLindex values) is suggested from the multispectral dataset within Argyre Mons, but the spectral resolution is too limited for a definitive mineral identification. This detection would coincide with the layers shown on Fig. 4.

4. Discussion

4.1. Origin of Argyre Mons

Volcanic landforms are abundant on Mars and display a diversity of constructional styles and sizes from the largest Olympus Mons shield structure (diameter ~600 km), to sub-kilometer scale pits and cones (e.g. Hodges and Moore, 1994; Farrand et al., 2005; Brož and Hauber, 2012). Given the overall size and physiography of Argyre Mons, along with other evidence for volcanism and magma-volatile interaction in the vicinity, we interpret the feature to be a remnant volcanic construct. Jovis Tholus (18.41°N, 242.59°E) provides an example of a shield structure (Plescia, 1994; Robbins et al., 2011) of comparable vertical and horizontal dimensions with a complex caldera structure similar in scale to the central depression of Argyre Mons (Fig. 16). Robbins et al. (2011) identified seven distinct, nested calderas with modeled surface ages based on crater counts ranging from 400 Ma to over 2 Ga. The relatively large size of the caldera complex relative to the total shield diameter is interpreted by Plescia (1994) to results from relatively large magma chambers at shallow depth.

Morphologically, Argyre Mons resembles other volcanic features elsewhere in the solar system. For example, the Ngorongoro Crater in the Arusha province of northern Tanzania is a volcanic shield structure and caldera of comparable size to Argyre Mons and is one of nine Plio-Pleistocene volcanoes that comprise the Ngorongoro Volcanic Highlands (NVH) complex of the East African Rift System (Fig. 17a). The $^{40}Ar/^{39}Ar$ ages constrain Ngorongoro volcanism to 2.25 ± 0.02 Ma to 2.01 ± 0.02 Ma (Mollel et al., 2008), and geochemical and geophysical evidence suggests the volcanism of the complex is attributable to one or more mantle plumes (Mechie et al., 1997; Ebinger and Sleep, 1998; Rogers et al., 2000; Mollel et al., 2008).

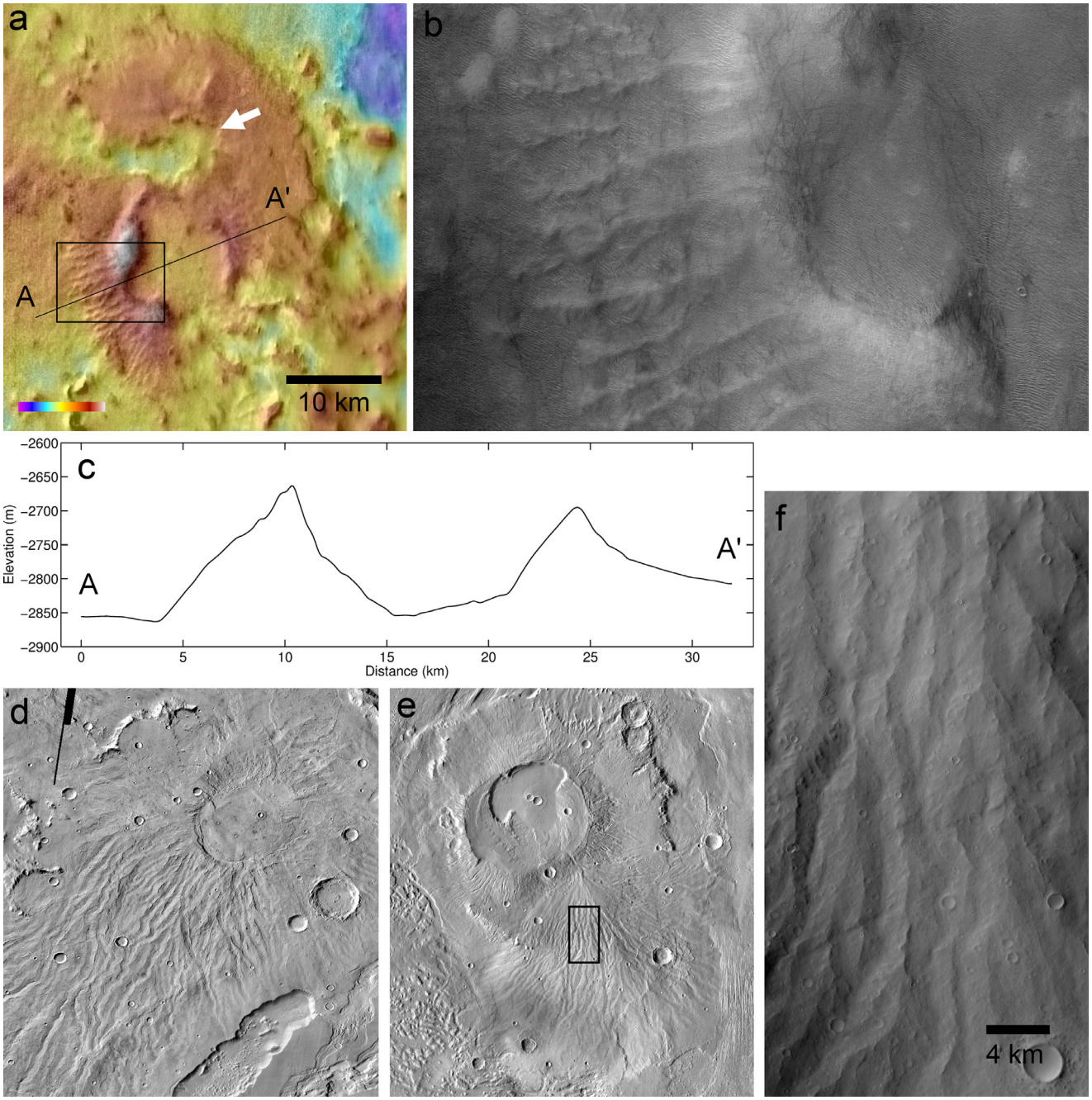

Fig. 13. (a) MOLA color topography with the daytime THEMIS IR mosaic used for shading showing a possible remnant of a volcanic edifice with irregular caldera and alternating ridges and gullies creating a ribbed texture on the flanks. The location of (a) is shown in Fig. 9. Box shows location of (b) and the ground track of topographic profile A – A′ in (c). White arrow points to the headwall of a channel etched into the plateau. (b) Western flank of candidate volcano highlighting alternating ridge and trough topography. Ridges are spaced ~1 km apart. (CTX image: G15_023964_1319_XI_48S046W). (c) Topographic profile across feature in (a). (d) Hadriacus Mons and (e) Apollinaris Mons (THEMIS daytime mosaic). See Fig. 1a for context. Box shows location of (f). (f) Alternating ridge and trough morphology on fan of Apollinaris Mons (CTX image: P02_001988_1709_XI_09S185W). (For interpretation of the references to colour in this figure legend, the reader is referred to the web version of this article.)

Doom Mons on Saturn's moon Titan (Fig. 17b), ~70 km in diameter and 1.45 ± 0.2 km high, is similar in size to Argyre Mons and has been interpreted as possibly an eroded cryovolcanic shield or dome (Lopes et al., 2013) providing an additional morphological analog. The mountain is adjacent to Sotra Patera, an elongated pit ~30 km in diameter and 1.7 ± 0.2 km deep. The morphological similarities between cryovolcanic and basaltic volcanic features have been explained by *Kargel* et al. (1991) as due to cryovolcanic mixtures such as ammonia-water behaving much as basaltic volcanism does on Earth, with comparable construction of low-profile volcanic shields and other constructional volcanoes and flow fields.

Mt. Sidley in Antarctica has parasitic vents near the margin of its southern flank and layered pyroclastic and sedimentary deposits, including finely-bedded epiclastic and hyaloclastic deposits containing pumice-rich layers. Mt Sidley is thought to have formed in sub-ice conditions and experienced an explosive proximal eruption and catastrophic landslide of its southern flank to form a large breached caldera exposing the volcanic strata within its interior (Panter et al., 1994) (Fig. 17c).

Sub-ice volcanism for Argyre Mons would be consistent with the geologic mapping investigation of Dohm et al. (2015) showing that the youngest basin unit (unit HAb4a) posses esker-like

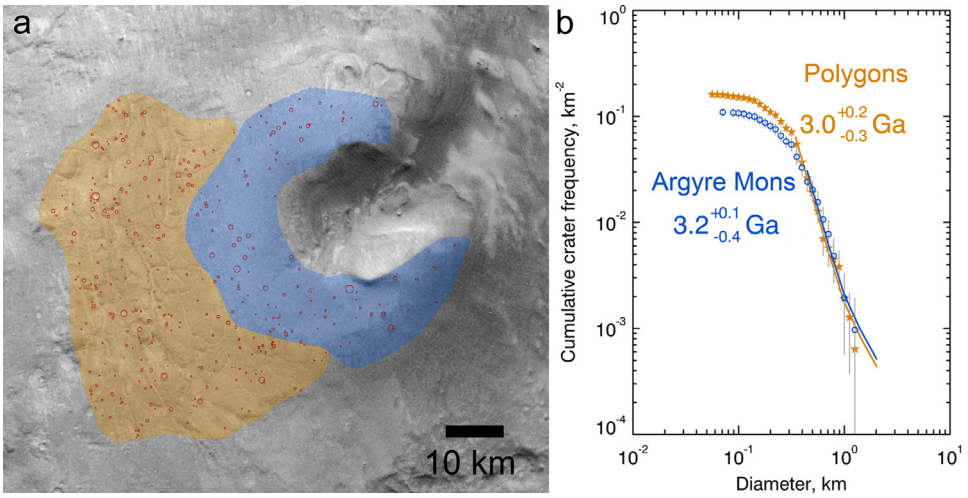

Fig. 14. (a) Crater count areas on the flanks of Argyre Mons (blue: 1033 km^2) and area of giant polygons (orange: 1574 km^2) with the measured craters outlined in red. (b) Cumulative crater-size frequency distribution of craters on the flanks of Argyre Mons (blue) and the giant polygons (orange). Absolute model ages are estimated using crater diameter ranges 0.35 – 2 km (orange) and 0.45 – 2 km (blue). (For interpretation of the references to colour in this figure legend, the reader is referred to the web version of this article.)

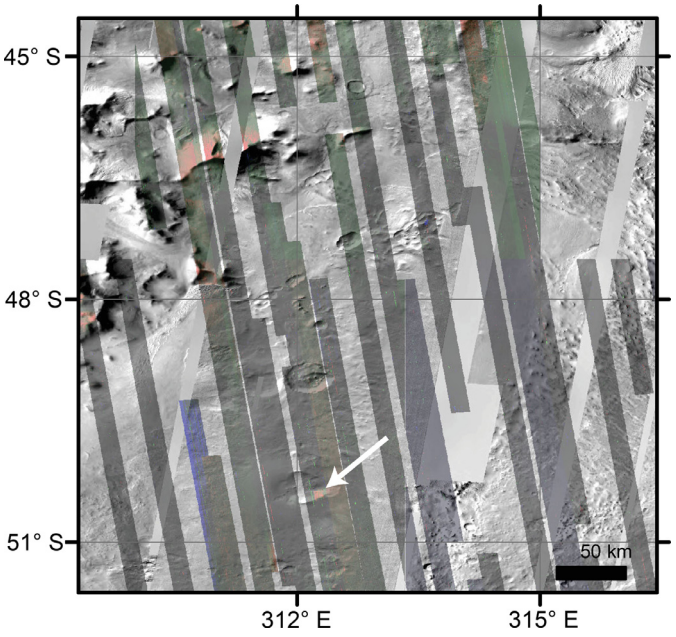

Fig. 15. RGB composite of CRISM summary parameters (R = OL index, G = LCP index, B = HCP index) of multispectral tiles 0291, 0292 and 0361 projected in transparency over the THEMIS IR day mosaic. Olivine detections are highlighted in red. The white arrow points at the location of putative olivine or clay detections within Argyre Mons, which have to be confirmed with hyperspectral observations. (For interpretation of the references to colour in this figure legend, the reader is referred to the web version of this article.)

ridges indicative of ice deposits (Hiesinger and Head, 2002; Kargel, 2004; Banks et al., 2009). The estimated absolute range of formation ages for this unit is ~3.5 to ~1.3 Ga based on crater counts that included partially buried craters and only pristine superposed craters respectively. This overlaps with the ~3 Ga estimated age for Argyre Mons and the adjacent giant polygons (Section 3.5). If the giant polygons in fact indicate substantial liquid water or ice, their discovery within Argyre basin has implications for its geologic history and would bolster the hypothesis that the basin contained a lake or ice sheet at some point in its past (Dohm et al. 2015). If a transient lake resulted from Tharsis-driven activity, as hypothesized by Dohm et al. (2015), then the lake may have frozen with subsequent formation of Argyre Mons in an ice body, and thus explaining the morphologic expression which compares to Mt Sidley that developed in an ice sheet in the Antarctic.

Tanaka (2000) mapped much of the floor of Argyre basin as etched plains deposits and attributed its etched appearance, primarily east of the area studied here, to eolian deflation of fine-grained, poorly indurated material. Kerber et al. (2012) concluded that floor materials were not likely derived from volcanism, as suggested for several other occurrences of friable deposits on Mars believed to result from volcanic ash fall (e.g. Grant and Schultz, 1990; Moore, 1990; Grant et al., 2010). This conclusion was based on the results of modeling pyroclastic airfall dispersal which did not suggest Argyre to be a likely place for pyroclastic deposits. Volcanism at and around Argyre Mons, however, would provide a local source for volcanically derived materials, making pyroclastic deposits a viable candidate for the source of the etched terrains within the basin.

The observation of other possible volcanic features and other landforms indicative of endogenic modification of the basin floor materials supports a volcanic interpretation for Argyre Mons. The numerous cavi, pits and rimmed depressions have morphologic similarities to volcanic features on Earth and elsewhere on Mars. Faults and collapse depressions are associated with volcanism and are especially prevalent in the Tharsis and surrounding regions related to the development of the prominent magmatic center of activity. Examples include structurally-controlled elongated depressions in the Tempe Terra plateau (Scott and Dohm, 1990), structurally-controlled collapse features and channels in the Thaumasia region (Dohm et al., 2001), and widely distributed pit crater chains on Tharsis (Wyrrick et al., 2004; Ferrill et al., 2004). Memnonia and Sirenum faults extend from Tharsis and cut the large north-trending basins of Terra Sirenum, many of which accompany collapse depressions and valley networks, as well as source Mangala Valles (Anderson et al., 2016). Such activity, which resulted in the formation of Mangala Valles, may have included the emplacement of dikes which breached the cryosphere and released confined groundwater (Head and Wilson, 2002; Wilson and Head, 2002).

Many of the rocky mounds and ridges observed within the cavi (Section 3.2) have a layered appearance or are coarsely terraced with distinctly-flat surfaces or ridges (Fig. 10b, c), similar to the layered intrusions and flood basalts proposed to comprise the wall rocks of Valles Marineris (McEwen et al., 1999;

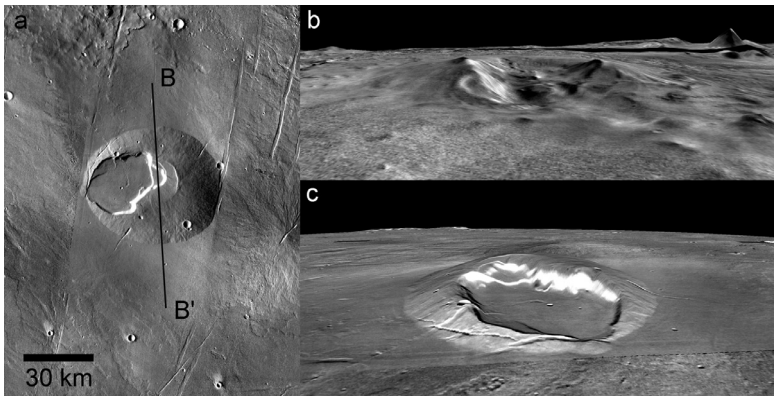

Fig. 16. (a) THEMIS IR daytime mosaic of Jovis Tholis and perspective views of the THEMIS mosaic draped on MOLA topography of (b) Argyre Mons looking west and (c) Jovis Tholis looking east at the same scale. The black line and label is the ground track of the topographic profile B – B′ across Jovis Tholis in Fig. 20. Location of Jovis Tholus and Argyre Mons shown in Fig. 1a.

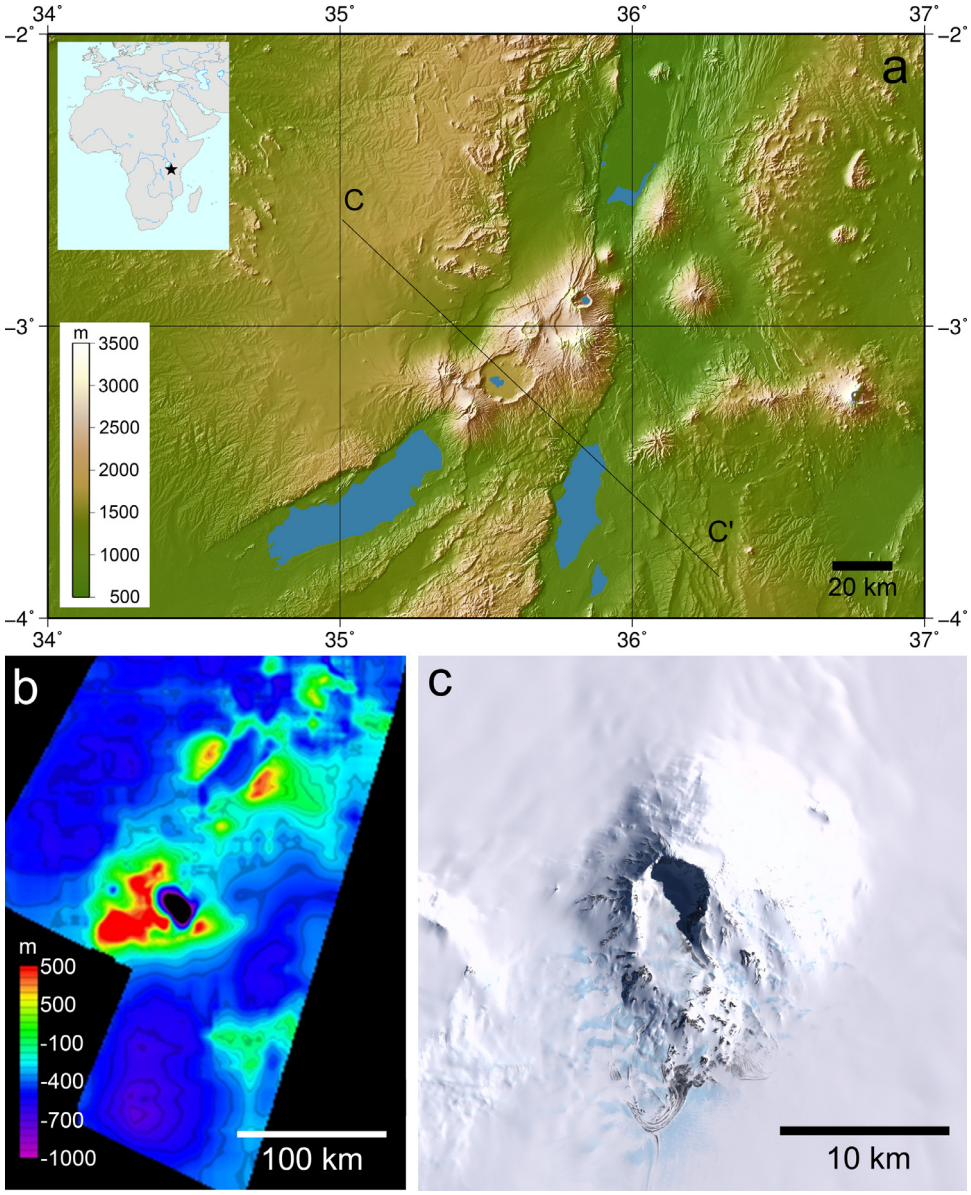

Fig. 17. (a) Shuttle Radar Topography Mission (SRTM) (Slater et al., 2006; Farr et al., 2007) version 2 DEM at 3 arc second resolution of the Ngorongoro Volcanic Highlands complex, Tanzania (3.20°S, 35.46°E). Ngorongoro Crater is a ~20 km wide, well preserved caldera (~ 2 Ma). Black line: ground track and label of topographic profile in Fig. 20. (b) Cassini Synthetic Aperture Radar derived DTM of the Dom Mons and Soltra Patera region (Lopes et al., 2013). (c) Portion of USGS Landsat Image Mosaic of Antarctica (LIMA) Natural Color Pan derived from Landsat 7ETM+ bands 3, 2, and 1 of Mt Sidley, Antarctica.

Williams et al., 2003); they could be exposed intrusive-bodies (plutons, dikes and sills) or deposits resulting from phreatomagmatic eruptions. The southwest rim of one of the larger cavi appears to have been breached by liquid water as it is notched with a channel extending down its exterior flank (Fig. 10d), indicating that melting played a role in the cavi formation. The adjacent large mound, with a basal diameter of ~2 km and extending ~0.5 km above the depression floor, could be a remnant intrusive body resulting from magma that intruded into and destabilized the overlying icy terrain resulting in the formation of the cavi.

Other pits, cones, and rings of material may be analogous to tuff cones and maars (Fig. 11d and e). On Earth, maars are broad, low-rimmed hydrovolcanic craters with deposits that may contain little or no magmatic material. Pits and graben on Alba Patera have been interpreted to be maars (Mège and Masson, 1996) but generally there has been a lack of identification of maars on Mars.

The Pinacate volcanic field in Mexico provides an example of a concentration of cones and maars (Gutmann, 2002). Among the principal features of this region are Cerro Colorado, an elongated 1–3 km tuff cone, and Elegante crater, a 1.6 km wide maar (Fig. 11f). The largest known maars on Earth, the Espenberg Maars on the Seward Peninsula in northwest Alaska, are 4–8 km in diameter and resulted from a series of basaltic eruptions through thick permafrost (Begét et al., 1996). The explosive eruptions, resulting from the contact between the magma and the small amount of melt-derived water, excavated ~300 m deep craters. The phreatomagmatic eruptions that formed the Ukinrek Maars in Alaska in 1977 were observed and documented with intense phreatomagmatic activity lasting several days (Fig. 11g) (Kienle et al., 1980; Self et al., 1980). Two of the largest terrestrial volcanic tuff cones, the Menan Buttes in the Snake River Plain of southeast Idaho (Fig. 11h), are part of a late-Pleistocene complex of basaltic tuff cones (Hughes et al., 1999) formed by a basaltic dike intruding into shallow water-saturated alluvium forming cones of lapilli-size particles of volcanic glass altered by water (Hamilton and Myers, 1963; Russell and Brisbin, 1990). They reach an elevation ~250 m above the surrounding plains with base diameters ~4 km in the widest dimensions. Tuff rings and cones have been tentatively identified in the Amenthes region of Mars (Brož and Hauber, 2013) with the larger cones of similar scale to the Menan Buttes.

Could some of these features, including Argyre Mons, alternately have formed as a result of a non-volcanic process? The water-rich, depositional history of the basin makes mud volcanism an attractive formation hypothesis (Dohm et al., 2015). Pitted cones, rings, and mounds can be generated through mud volcanism or the formation of ice mounds and pingos. Fluid expulsion in compacting deposits has been recognized to form volcano-like mounds in terrestrial sedimentary basins, both onshore and off-shore (Dimitrov, 2002; Kholodov, 2002; Kopf, 2002; Evans et al., 2008; Mazzini, 2009; Bonini and Mazzarini, 2010; Bonini, 2012). Pore fluid pressure builds when the pressure cannot dissipate adequately through the sediment and can be focused through fractures or zones of enhanced permeability to breach the capping layer. The extrusion of fluid and entrained sediments can result in a cone-shaped edifice, or mud volcano. Such a formation mechanism has been proposed for many of the mounds observed in the lowlands of Mars (Tanaka, 1997; Ferrand et al., 2005; Skinner and Mazzini, 2009; Oehler and Allen, 2010; Pondrelli et al., 2011; Komatsu et al., 2011; Allen et al., 2013) and within Valles Marineris (Okubo, 2016). Mud volcanism has also been associated with kilometer-scale polygons in the northern lowlands of Mars and off-shore sedimentary basins on Earth (McGowan, 2009, 2011; Allen et al., 2013).

Argyre Mons is significantly larger than other candidate mud volcanoes observed on Mars or any mud volcanoes identified on Earth (Fig. 18). The Touragai Mud volcano in eastern Azerbaijan is considered to be one of the largest onshore mud volcanoes, with an estimated 343 million cubic meters of mud breccia reaching a diameter between 2900 and 3200 m and a height of 500 m (Mazzini, 2009; Bonini, 2012), though mud volcanoes are typically much smaller than this. Argyre Mons by comparison is an order-of-magnitude wider making it an unlikely candidate to be the result of mud volcanism due to its sheer size and the required volume of sedimentary fine material.

Mud volcanism remains a reasonable possibility for the small cones and domical features observed north of Argyre Mons near the basin margin as discussed in Section 3.2 and highlighted in Fig. 12. Alternately, the formation of ice mounds and pingos can result in features with similar morphologies. Pingos form through the injection and freezing of pressurized water. As an ice mound grows, the surface ruptures over the ice core. The exposed ice can melt or sublime forming pits at or near the summit generating a morphology that can be similar to rootless cones (Flemal, 1976). Candidate pingos have been identified in several locations on Mars (e.g. Dundas et al., 2008; Burr et al., 2009; Dundas and McEwen, 2010; Soare et al., 2013) including areas around the Argyre basin rim (Soare et al., 2014a).

Image resolution is a limiting factor in distinguishing the nature of these features and thus their interpretation is equivocal. Rootless cones, mud volcanism, and pingo formation all indicate the presence of surface or near-surface water and contributes to the hypothesis that Argyre basin experienced extensive hydrologic activity through time, albeit likely punctuated (Hiesinger and Head, 2002; Soare et al., 2014a; Dohm et al., 2015).

An additional hypothesis for Argyre Mons is that rather than being a constructional feature, it is the result of an impact or a remnant erosional feature. The irregular, horseshoe-like shape of the edifice could be partly due to differential erosion or the result of formation from an oblique impact. Fig. 19 shows an unnamed crater north of Hellas basin with a similar width to the central depression of Argyre Mons. The high relief of the flanks and rim around the central depression of Argyre Mons would require $\gtrsim$ 500 m of deflation of the surrounding basin floor relative to the rim structure if it initially had a similar topographic expression as the elliptical crater as seen in the topographic profiles shown in Fig. 20. If the rim of the feature represents the approximate elevation of the basin floor surface at the time of an impact, i.e. the basin floor was ~500 m higher than the present-day level; this would require a removal of $\sim 3.8 \times 10^{14}$ m^3 of material from the basin interior. Eolian activity on the basin floor is evident with deflation and accumulation of dunes modifying the basin floor (Hiesinger and Head, 2002; Dohm et al., 2015); however evidence for the erosion and transport of such a large volume of material has not been reported.

4.2. Timing of endogenic activity

The region north of Argyre Mons containing the cavi and other tectonic and volcanic features (Figs. 10–12) has a near absence of craters indicating the current rate of deflation or modification of the surface must be rapid relative to the production rate of craters. The lack of craters precludes the determination of any model crater-retention age, however the preservation of the morphology of the cavi and other volcanic features despite a resurfacing rate that must be rapid relative to the formation rate of craters, implies these features must be relatively young. Resurfacing from the redistribution of polar ices resulting from the quasi-periodic variations in spin-axis obliquity (Laskar et al., 2004), could have engendered the atmospheric precipitation of ice/snow, the high to mid-latitudinal deposition and accumulation of ice/snow at the surface, and the formation of a meters- to decameters-thick mantle (Mustard et al., 2001; Head et al., 2003). Periglacial terrain has been reported in other parts of the Argyre basin above the floor

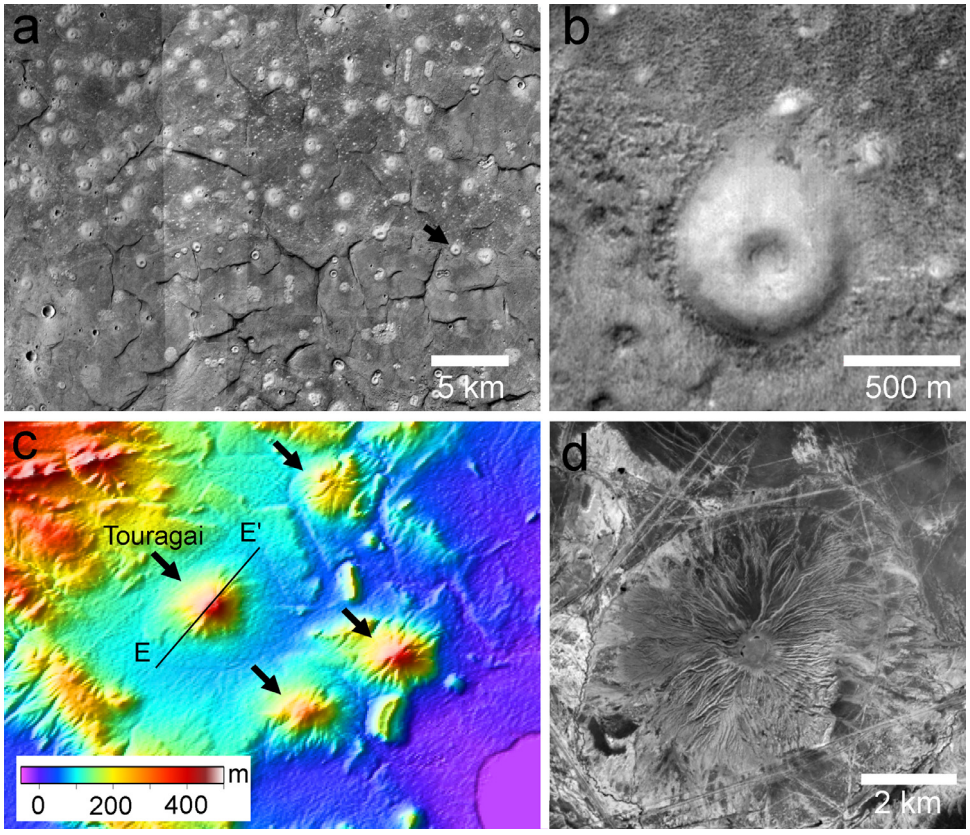

Fig. 18. Examples of mud volcanoes in Acidalia Planitia, Mars (a-b) and Azerbaijan, Earth (c-d). (a) Portions of CTX images B21_017950_2211_XN_41N026W and P19_008522_2211_XN_41N027W centered on 332.8°E, 40.6°N. (b) Portion of CTX image B21_017950_2211_XN_41N026W. (c) SRTM version 2 DEM at 3 arc second resolution of east Azerbaijan (lat: 40.05°N to 40.25°N, lon: 49.20°E to 49.45°E). Black arrows show locations of mud volcanoes. Black line shows ground track and label of topographic profile E – E′ in Fig. 20. (d) Portion of LANDSAT 8 [Irons et al., 2012] Operational Land Imager (OLI) panchromatic (band 8) image LC81660322013145LGN00 of Touragai, one of the largest terrestrial mud volcanoes.

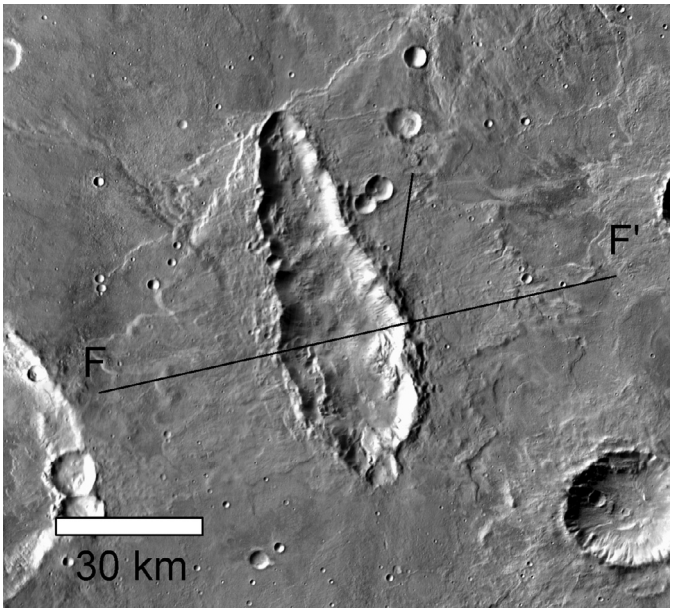

Fig. 19. THEMIS IR daytime mosaic of an unnamed elliptical crater (54.7°E, 21.1°S). Black line: ground track and label of topographic profile F – F′ in Fig. 20.

(Soare et al., 2014a,b, 2017) and we observe glacial-like landforms on the flanks of mountains located along the northwest margin of the basin floor indicating ice at or near the surface and highlight recent atmospheric deposition of ice in the region (Fig. 21). Glacier-like landforms, concentrated at mid-latitudes on Mars, are remnants of Late Amazonian Epoch ice ages (Head et al., 2003; Souness et al., 2012; Hubbard et al., 2014). Prior to 5 Ma, Mars is thought to have experienced a period of high (mean-polar) summer insolation; with an average obliquity of ~36°, this could have resulted in widespread glaciation at lower latitudes. If the observed surface in Argyre is a remnant of an icy mantle from a recent past obliquity excursion, its disruption by extensional tectonics and collapse by thermal destabilization to form cavi and explosive cratering (maars) by the near-surface intrusion of magma, would have occurred recently (several Myrs or less). Endogenic activity within the basin floor may therefore have been long lived, extending from the Late Hesperian/Early Amazonian with the construction of Argyre Mons, to the formation of the cavi, faults, and other volcanotectonic features that disrupted possible icy surfaces related to recent obliquity excursions.

4.3. Implications for astrobiology

Evidence for volcanism within the floor of Argyre basin, coupled with the basin's water-rich past, makes Argyre a site of enhanced astrobiological significance (Fairén et al., 2016) as the combination of crustal materials (including possible feldspathic and felsic basement materials (Wray et al., 2013; Sautter et al., 2015)) derived from far-reaching provenances, basaltic volcanic materials, liquid water, and hydrothermal activity resulting from volcano-ice interaction can potentially provide all the necessary ingredients for life. This suggests that the nearly 4 billion year old Argyre basin might have been a suitable region for the origin and early evolution of life at a time when Mars was still a water-rich planet. However,

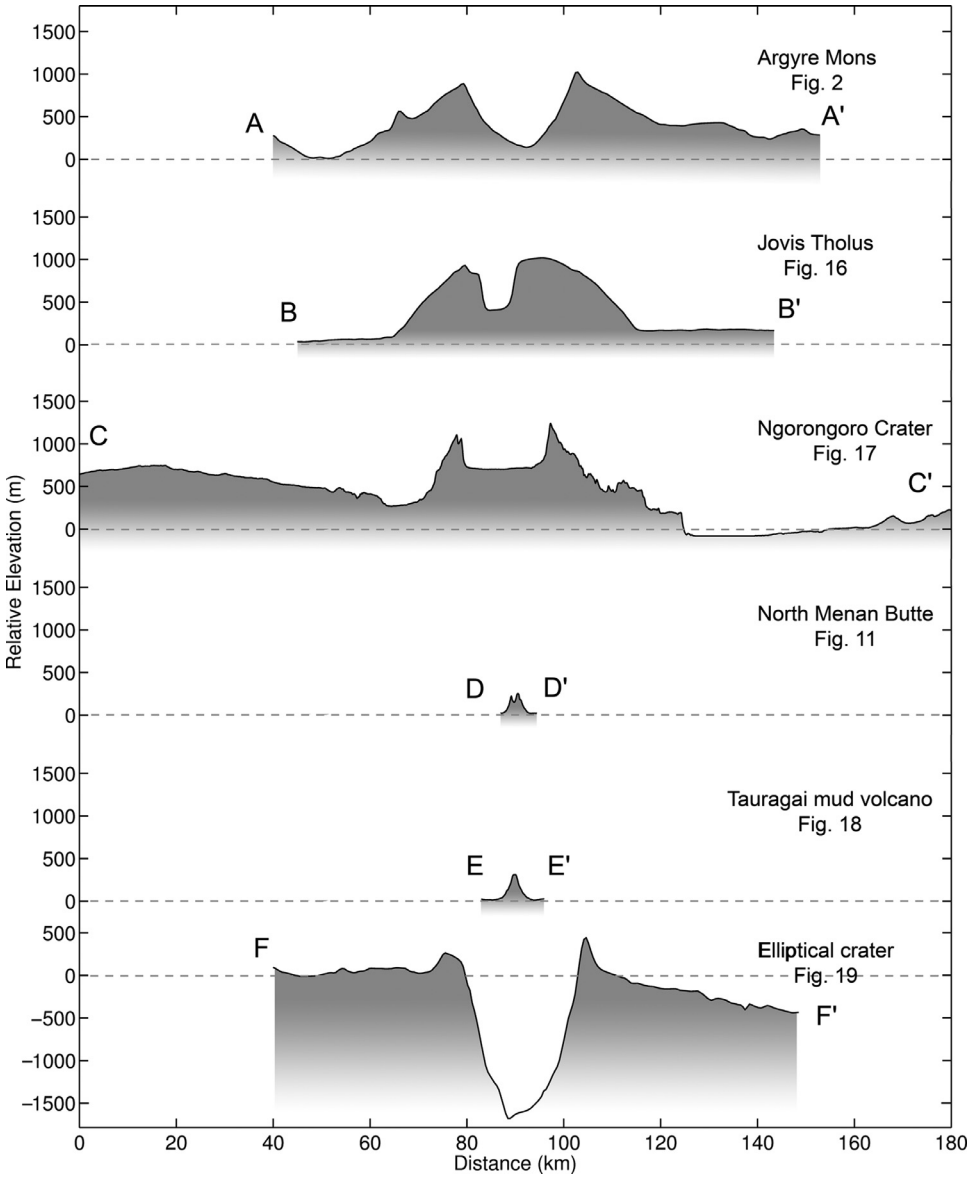

Fig. 20. Elevation profiles of Argyre Mons and possible analogs with reference figures labeled.

even if life did not originate independently in the region or anywhere else on Mars, microbes would have found habitable conditions in the Argyre basin if they arrived per asteroid exchange from Earth during the late heavy bombardment. This extensive region with a diameter >1200 km and a depth >4 km would have provided a diverse range of potential habitats with the presence of stable liquid water, and a continuum of geochemical and thermal gradients.

As Mars became colder and dryer through subsequent time periods, volcanism and magmatism could have maintained habitable conditions in the Argyre basin, at least in some locations, and may have represented one of the final outposts for ecosystem development on Mars. The existence of aquatic habitats in different places on Mars during the Noachian and into the Hesperian, up to 3 Gyr ago, is well established (see i.e., Fairén, 2010; Fairén et al., 2010; Dohm et al., 2011) and environmental conditions during the Amazonian have been historically regarded as too arid to support life. However, our investigation presented here support that magma-ice interactions occurred in the relatively recent past, as suggested by the relatively pristine appearance of cavi, possible maars and dikes, and other endogenically derived features north of Argyre Mons, coupled with a general lack of superposed craters. The intrusion of magma at the basal ice-substrate contact would have heated and melted the globally-continuous cryosphere and possible remaining glacial deposits, promoting the destabilization of the thick permafrost and the fracturing of the surface, allowing the release of pressurized groundwater in multiple phases. The melt water released from the glacier could have formed jökulhlaups and deposited sediments and ice across sandur plains.

The combination of subglacial lava flows (geothermal heat) and thick permafrost (source of liquid water) would have created subaerial and subsurface environments suitable for life development, as is observed from analog sites on Earth (Skidmore et al., 2000; Björnsson, 2003; Gilichinsky et al., 2004; Cousin and Crawford, 2011). These sites include subglacial caldera lakes (above the volcanic caldera but beneath the glacier surface), ice cave networks (when the meltwater is released at the edge of the glacier), or the subglacial basaltic lava edifice itself. The interaction between geothermal heat flow and an overlying cryosphere is conducive to the generation of hydrothermal systems (Schulze-Makuch et al., 2007), and meltwater cycles through the basaltic edifice and mixes with hydrothermal fluids. The usual inhabitants of these environ-

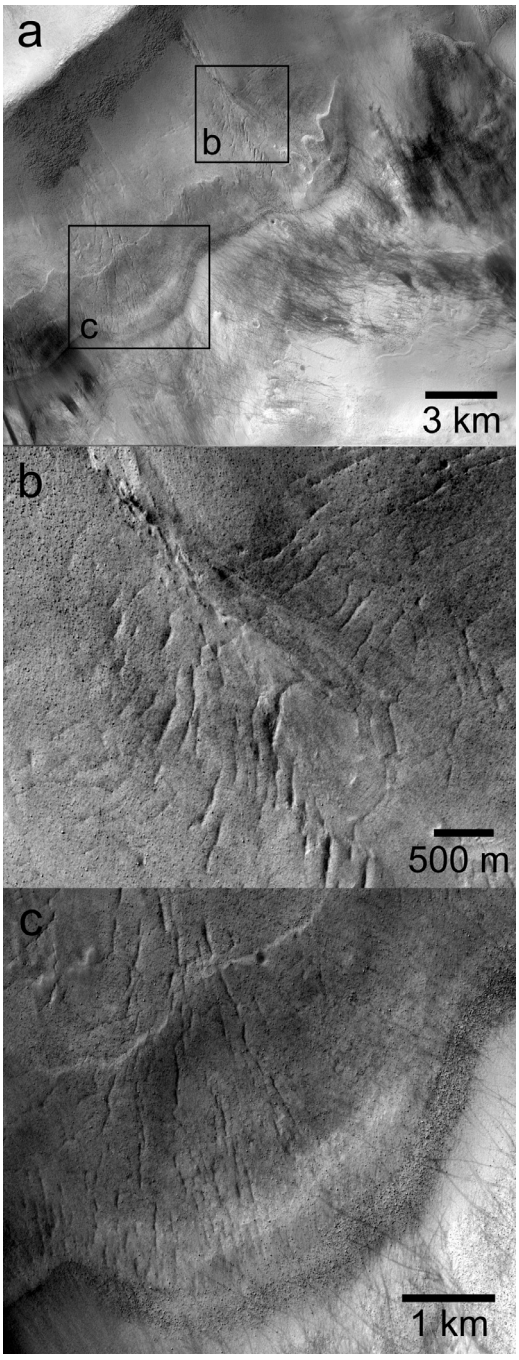

Fig. 21. (a) Portion of CTX image P13_006150_1323_XN_47S048W showing a glacier-like feature on the flank of a mountain at the margin of the Argyre basin floor. Black boxes are locations of image enlargements of subframes (b) and (c). See Fig. 9 for context. (b) Glacier surface at a gully entrant. Gully formation in the headwall appears to influence the orientation of the crevasses where they are longitudinally oriented, indicating lateral expansion, and transition to transverse orientations at increasing distance from the gullies. (c) Glacier surface showing longitudinal and splay crevasses and the terminus marked with a moraine comprised of a dense accumulation of large boulders.

ments are chemotrophic microbial communities tolerant of oligotrophic conditions, low temperatures and high pressures, exploiting the cold basaltic and hydrothermal settings and using sulfide, sulfur or hydrogen as electron donors, and oxygen, sulfate or CO_2 as electron acceptors (Gaidos et al., 2009).

Mud volcanism might have also occurred in the Argyre basin, possibly associated with hydrothermal systems, providing an intriguing site for a future lander or rover mission, as a means to access the subsurface and possibly sample fossilized microbes. Analog sites from Earth indicate that mud volcanism is often associated with microbial life (Yakimov et al., 2002; Mahaney et al., 2004; Niemann et al., 2006; Schulze-Makuch et al., 2011).

The apparent contemporaneous age and location of giant polygons and a sizeable volcanic feature provided the possibility for steep thermal and geochemical gradients involving the presence of liquid water in Argyre and possible continued magma-ice interactions would have provided an oasis for life in an otherwise desiccated planet, relying on particular local geological conditions without the need to invoke global events such as variations in orbital parameters (Forget et al., 2006). Therefore, local conditions at Argyre could have significantly expanded the martian habitability window beyond the Hesperian period, and this window of habitability might have closed relatively recently, or may still be open, providing the possibility to retrieve extant life. We suggest that the search for relatively recent aqueous environments at Argyre as repositories of possible evidence of martian life should be a priority target for the further astrobiological exploration of Mars (Fairén et al., 2016).

5. Conclusions

We have identified numerous landforms that suggest that past volcanic, tectonic, and hydrologic activity occurred within the floor of the Argyre basin. This study focused on the most prominent feature, Argyre Mons, a ~50 km wide structure, and the adjacent terrain in the northwest portion of the basin floor. Based on the morphology and size of Argyre Mons, we conclude that it is likely a degraded shield structure. This interpretation is strengthened by the observations of additional features with morphologies suggestive of volcanism and tectonism within the region. How widespread the volcanic active was throughout the basin remains unclear. The size-frequency distribution of craters superposed on Argyre Mons yields a model age ~3 Ga. However, the relatively pristine appearance of cavi, possible maars, and other endogenically derived features north of Argyre Mons, coupled with a general lack of superposed craters, implies magma-ice interaction occurred in the relatively recent past suggesting that volcanism has persisted in Argyre Planitia over an extended period of time.

These observations represent a previously unrecognized aspect of the geologic history of the basin and the accumulated material within the basin, at least 2 km in thickness (Dohm et al., 2015), is likely composed partially of material of volcanic origin. Like the long-lived volcanic centers of Elysium, Tharsis, and the region that straddles them, which includes Late Amazonian activity (Dohm et al., 2008), Argyre may have also been a center of volcanic activity initiating at least as far back as the Early Amazonian and continuing up until very recent time. This may have been obscured by the fact that volcanism has had to compete with deposition, glaciations, and other geologic processes which have occurred with greater intensity within a large basin that has been a sink for sediments and volatiles during extended time periods.

Acknowledgments

We thank Randy Kirk and his group at the USGS Flagstaff for providing the Titan DEMs, and the two anonymous reviewers for helpful and constructive comments that improved the manuscript. J.-P.W. and A.P. were supported by a NASA Mars Data Analysis Program Grant No. NNX14AM12G. A.G.F. was supported by the Project "icyMARS", European Research Council Starting Grant no 307496. D.S.-M. was supported by ERC Advanced Grant 339231 (HOME). Part of this work was carried out at the Jet Propulsion Laboratory, California Institute of Technology, under contract with NASA.

References

Allen, et al., 2013. Fluid expulsion in terrestrial sedimentary basins: a process providing potential analogs for giant polygons and mounds in the martian lowlands. Icarus 224, 424–432.

Anderson, R.C., Dohm, J.M., Robbins, S., Schroeder, J., 2016. Completion and submission of the Terra Sirenum map project. Annual Planetary Geologic Mappers Meeting.

Banks, M.E., et al., 2009. An analysis of the sinuous ridges in the southern Argyre Planitia, Mars using HiRISE and CTX images and MOLA data. J. Geophys. Res 114, E09003. http://dx.doi.org/10.1029/2008JE003244.

Begét, J.E., Hopkins, D.M., Charron, S.D., 1996. The largest known maars on Earth, Seward Peninsula, northwest Alaska. Arctic 49, 62–69.

Bernhardt, H., Hiesinger, H., Reiss, D., Ivanov, M., Erkeling, G., 2013. Putative eskers and new insights into glacio-fluvial depositional settings in southern Argyre Planitia, Mars. Planet. Space Sci. 85, 261–278.

Björnsson, H., 2003. Subglacial lakes and jökulhlaups in Iceland. Global Planet. Change 35, 255–271.

Bonini, M., Mazzarini, F., 2010. Mud volcanoes as potential indicators of regional stress and pressurized layer depth. Tectonophysics 494, 32–47.

Bonini, M., 2012. Mud volcanoes: indicators of stress orientation and tectonic controls. Earth-Sci. Rev. 115, 121–152.

Brož, P., Hauber, E., 2012. A unique volcanic field in Tharsis, Mars: pyroclastic cones as evidence for explosive eruptions. Icarus 218, 88–99.

Brož, P., Hauber, E., 2013. Hydrovolcanic tuff rings and cones as indicators for phreatomagmatic explosive eruptions on Mars. J. Geophys.Res. 118, 1–20. doi:10.1002/jgre.20120.

Buczkowski, D.L., Seelos, K.D., Cooke, M.L., 2012. Giant polygons and circular graben in western Utopia basin, Mars: exploring possible formation mechanisms. J. Geophys. Res. 117, E08010. doi:10.1029/2011JE003934.

Burr, D.M., Tanaka, K.L., Yoshikawa, K., 2009. Pingos on Earth and Mars. Planet. Space Sci. 57, 541–555.

Carr, M.H., Clow, G.D., 1981. Martian channels and valleys: their characteristics, distribution, and age. Icarus 48, 91–117.

Carter, J., Poulet, F., Bibring, J.P., Mangold, N., Murchie, S., 2013. Hydrous minerals on Mars as seen by the CRISM and OMEGA imaging spectrometers: updated global view. J. Geophys. Res. 118, 831–858.

Christensen, P.R., Jakosky, B.M., Kieffer, H.H., Malin, M.C., McSween Jr., H.Y., Nealson, K., Mehall, G.L., Silverman, S.H., Ferry, S., Caplinger, M., Ravine, M., 2004. The Thermal Emission Imaging System (THEMIS) for the Mars Odyssey mission. Space Sci. Rev. 110, 85–130.

Cooke, M., Islam, F., McGill, G., 2011. Basement controls on the scale of giant polygons in Utopia Planitia, Mars. J. Geophys. Res. 116, E09003. doi:10.1029/2011JE003812.

Cousins, C.R., Crawford, I.A., 2011. Volcano-ice interaction as a microbial habitat on Earth and Mars. Astrobiology 11 (7), 695–710.

Dimitrov, L.I., 2002. Mud volcanoes—the most important pathway for degassing deeply buried sediments. Earth-Sci. Rev. 59, 49–76.

Dohm, J.M., et al., 2001. Ancient drainage basin of the Tharsis region, Mars: potential source for outflow channel systems and putative oceans or paleolakes. J. Geophys. Res. 106, 32942–32958 doi:101029/2000JE001468.

Dohm, J.M., et al., 2008. Recent geological and hydrological activity on Mars: the Tharsis/Elysium corridor. Planet. Space Sci. 56, 985–1013.

Dohm, J.M., et al., 2009. New evidence for a magmatic influence on the origin of Valles Marineris, Mars. J. Volcanol. Geotherm. Res. 185, 12–27.

Dohm, J.M., et al., 2011. An inventory of potentially habitable environments on Mars: geological and biological perspectives.. In: Garry, W.B., Bleacher, J.E. (Eds.). In: Analogs for Planetary Exploration, 483. Geol Soc Amer Spec Pap, pp. 317–347. doi:10.1130/2011.2483(21).

Dohm, J.M., Hare, T.M., Robbins, S.J., Williams, J.-P., Soare, R.J., El-Maarry, M.R., Conway, S.J., Buczkowski, D.L., Kargel, J.S., Banks, M.E., Fairén, A.G., Schulze–Makuch, D., Komatsu, G., Miyamoto, H., Anderson, R.C., Davila, A.F., Mahaney, W.C., Fink, W., Cleaves, H.J., Yan, J., Hynek, B., Maruyama, S., 2015. Geological and hydrological histories of the Argyre province, Mars. Icarus 253, 66–98.

Dundas, C.M., Mellon, M.T., McEwen, A.S., Lefort, A., Keszthelyi, L.P., Thomas, N., 2008. HiRISE observations of fractured mounds: possible Martian pingos. Geophys. Res. Lett. 35, L04201. doi:10.1029/2007GL031798.

Dundas, C.M., McEwen, A.S., 2010. An assessment of evidence for pingos on Mars using HiRISE. Icarus 205, 244–258.

El Maarry, M.R., et al., 2012. Searching for evidence of hydrothermal activity at Apollinaris Mons, Mars. Icarus 217, 297–314.

El Maarry, M.R., Dohm, J.M., Michael, G., Thomas, N., Maruyama, S., 2013. Morphology and evolution of the ejecta of Hale crater in Argyre basin, Mars: results from high resolution mapping. Icarus 226, 905–922.

Evans, R.J., Stewart, S.A., Davies, R.J., 2008. The structure and formation of mud volcano summit calderas. J. Geol. Soc. London 165, 769–780.

Fagents, S.A., Lanagan, P.D., Greeley, R., 2002. Rootless cones on Mars: A consequence of lava-ground ice interaction. In: Smellie, J.L., Chapman, M.G. (Eds.). In: Volcano-Ice Interaction on Earth and Mars, 202. Geol. Soc. Spec. Publ., pp. 295–317.

Fagents, S.A., Thordarson, T., 2007. Rootless volcanic cones in Iceland and on Mars. In: Chapman, M.G., Skilling, I.P. (Eds.), The Geology of Mars: Evidence from Earth-Based Analogues. Cambridge Univ. Press, New York.

Fairén, A.G., 2010. A cold and wet Mars. Icarus 208, 165–175.

Fairén, A.G., Davila, A.F., Lim, D., Bramall, N., Bonaccorsi, R., Zavaleta, J., Uceda, E.R., Stoker, C., Wierzchos, J., Amils, R., Dohm, J.M., Andersen, D., McKay, C., 2010. Astrobiology through the ages of Mars. Astrobiology 10, 821–843.

Fairén, A.G., Dohm, J.M., Rodríguez, J.A.P., Uceda, E.R., Kargel, J., Soare, R., Cleaves, H.J., Oehler, D., Schulze-Makuch, D., Essefi, E., Banks, M.E., Komatsu, G., Fink, W., Robbins, S., Yan, J., Miyamoto, H., Maruyama, S., Baker, V.R., 2016. The Argyre region as a prime target for in situ astrobiological exploration of Mars. Astrobiology 16, 143–158.

Farr, T.G., Rosen, P.A., Caro, E., Crippen, R., Duren, R., Hensley, S., Kobrick, M., Paller, M., Rodriguez, E., Roth, L., Seal, D., Shaffer, S., Shimada, J., Umland, J., Werner, M., Oskin, M., Burbank, D., Alsdorf, D., 2007. The Shuttle Radar Topography Mission. Rev. Geophys. 45, RG2004. doi:10.1029/2005RG000183.

Farrand, W.H., Gaddis, L.R., Keszthlyi, L., 2005. Pitted cones and domes on Mars: observations in Acidalia Planitia and Cydonia Mensae using MOC, THEMIS, and TES data. J. Geophys. Res. 110. http://dx.doi.org/10.1029/2004JE002297.

Ferrill, D.A., et al., 2004. Dilational fault slip and pit chain formation on Mars. GSA Today 14. doi:10.1130/1052-5173(2004)014⟨4,DFSAPC⟩2.0.CO;2.

Flahaut, J., Quantin, C., Clenet, H., Allemand, P., Mustard, J.F., Thomas, P., 2012. Pristine Noachian crust and key geologic transitions in the lower walls of Valles Marineris: insights into early igneous processes on Mars. Icarus 221, 420–435.

Flemal, R.C., 1976. Pingos and pingo scars: their characteristics, distribution, and utility in reconstructing former permafrost environments. Quaternary Res 6, 37–53.

Forget, F., Haberle, R.M., Montmessin, F., Levrard, B., Head, J.W., 2006. Formation of glaciers on Mars by atmospheric precipitation at high obliquity. Science 311, 368–371.

Gaidos, E., Marteinsson, V., Thorsteinsson, T., Johannesson, T., Rúnarsson, Á.R., Stefansson, A., Glazer, B., Lanoil, B., Skidmore, M., Han, S., Miller, M., 2009. An oligarchic microbial assemblage in the anoxic bottom waters of a volcanic subglacial lake. ISME J. 3, 486–497.

Ghent, R.R., Anderson, S.W., Pithawala, T.M., 2012. The formation of small cones in Isidis Planitia, Mars through mobilization of pyroclastic surge deposits. Icarus 217, 169–183.

Gilichinsky, D., Rivkina, E., Shcherbakova, V., Laurinavichuis, K., Tiedje, J., 2004. Supercooled water brines within permafrost—an unknown ecological niche for microorganisms: a model for astrobiology. Astrobiology 3, 331–341.

Goldspiel, J.M., Squyres, S.W., 2000. Groundwater sapping and valley formation on Mars. Icarus 148, 176–192.

Grant, J.A., 2000. Valley formation in Margaritifer Sinus, Mars, by precipitation-recharged ground-water sapping. Geology 28, 223–226.

Grant, J.A., Schultz, P.H., 1990. Gradational epochs on Mars: Evidence from west-northwestof Isidis basin and Electris. Icarus 84, 166–195.

Grant, J.A., Wilson, S.A., Noe Dobrea, E., Fergason, R.L., Griffes, J.L., Moore, J.M., Howard, A.D., 2010. HiRISE views enigmatic deposits in the Sirenum Fossaeregion of Mars. Icarus 205, 53–63.

Greeley, R., Fagents, S.A., 2001. Icelandic pseudocraters as analogs to some volcanic cones on Mars. J. Geophys. Res. 106 20,527–20,546.

Gulick, V.C., 1998. Magmatic intrusions and a hydrothermal origin for fluvial valleys on Mars. J. Geophys. Res. 103 19,365–19,388.

Gulick, V.C., 2001. Origin of the valley networks on Mars: a hydrological perspective. Geomorphology 37, 241–268.

Gutmann, J.T., 2002. Strombolian and effusive activity as precursors to phreatomagmatism: eruptive sequence at maars of the Pinacate volcanic field, Sonora, Mexico. J. Volcanol. Geotherm. Res. 113, 345–356.

Hamilton, W., Myers, W.B., 1963. Menan Buttes, cones of glassy basalt tuff in the Snake River Plain. U.S. Geological Survey Professional Paper, 450E, Idaho, pp. E114–E118.

Hartmann, W.K., 2005. Martian cratering 8: isochron refinement and the chronology of Mars. Icarus 174, 294–320.

Hauber, E., Brož, P., Rossi, A.P., Michael, G., 2015. A field of small pitted cones on the floor of Coprates Chasma Mars: volcanism inside Valles Marineris? *Lunar Planet. Sci. Conf.*, 46th Abstract 1476.

Head, J.W., Wilson, L., 2002. Mars: a review and synthesis of general environments and geological settings of magma H_20 interactions. In: Smellie, J.L., Chapman, M.G. (Eds.), Volcano–Ice Interaction on Earth and Mars. Geological Society, London, pp. 27–58. (Special publications 202.).

Head, J.W., Mustard, J.F., Kreslavsky, M.A., Milliken, R.E., Marchant, D.R., 2003. Recent ice ages on Mars. Nature 426, 797–802.

Hubbard, B., Souness, C., Brough, S., 2014. Glacier-like forms on Mars. Cryosphere 8, 2047–2061.

Hiesinger, H., Head, J.W., 2000. Characteristics and origin of polygonal terrain in southern Utopia Planitia, Mars: results from Mars orbiter laser altimeter and Mars orbiter camera data. J. Geophys. Res. 105, 11999–12022.

Hiesinger, H., Head, J.W., 2002. Topography and morphology of the Argyre basin, Mars: implications for its geologic and hydrologic history. Planet. Space Sci. 50, 939–981.

Hodges, C.A., Moore, H.J., 1994. Atlas of Volcanic Landforms on Mars. U.S. Professional Paper 1534, p. 194.

Howard, A.D., Kochel, R.C., Holt, H.E. (Eds.), 1988, Sapping Features of the Colorado Plateau. NASA SP-491.

Hughes, S.S., Smith, R.P., Hackett, W.R., Anderson, S.R., 1999. Mafic volcanism and environmental geology of the Eastern Snake River Plain, Idaho. In: Hughes, S.S., Thackray, G.D. (Eds.), Guidebook to the Geology of Eastern Idaho. Idaho Museum of Natural History, pp. 143–168.

Irons, J.R., Dwyer, J.L., Barsi, J.A., 2012. The next Landsat satellite: the Landsat Data Continuity Mission. Remote Sens. Environ. 122, 11–21.

Jaeger, W.L., Keszthelyi, L.P., McEwen, A.S., Dundas, C.M., Russell, P.S., 2007. Athabasca Valles, Mars: a lava-draped channel system. Science 317, 1709–1711.
Jaumann, R., et al., 2007. The High Resolution Stereo Camera (HRSC) experiment on Mars Express: instrument aspects and experiment conduct from interplanetary cruise through the nominal mission. Planet. Space Sci. 55, 928–952. http://dx.doi.org/10.1016/j.pss.2006.12.003.
Kargel, J.S., 2004. Mars: a Warmer Wetter Planet. Praxis-Springer, p. 557.
Kargel, J.S., Strom, R.G., 1992. Ancient glaciation on Mars. Geology 20, 3–7.
Kerber, L., Head, J.W., Madeleine, J.-B., Foget, F., Wilson, L., 2012. The dispersal of pyroclasts from ancient explosive volcanoes on Mars: Implications for the friable layered deposits. Icarus 219, 358–381.
Keszthelyi, L.P., et al., 2010. Hydrovolcanic features on Mars: preliminary observations from the first Mars year of HiRISE imaging. Icarus 205, 211–229.
Kholodov, V.N., 2002. Mud volcanoes, their distribution, regularities, and genesis: communication 1. Mud volcanic provinces and morphology of mud volcanoes. Lithol. Miner. Resour. 27, 197–209.
Kienle, J., Kyle, P.R., Self, S., Motyka, R.J., Lorenz, V., 1980. Ukinrek Maars, Alaska, I. April 1977 eruption sequence, petrology and tectonic setting. J. Volcano. Geotherm. Res. 7, 11–37.
Kneissl, T., van Gasselt, S., Neukum, G., 2011. Map-projection-independent crater size-frequency determination in GIS environments — New software tool for ArcGIS. Planet. Space Sci. 59, 1243–1254.
Komatsu, G., Ori, G.G., Cardinale, M., Dohm, J.M., Baker, V.R., Vaz, D.A., Ishimaru, R., Namiki, N, Matsui, T., 2011. Roles of methane and carbon dioxide in geological processes on Mars. Planet. Space Sci. 59, 169–181.
Kopf, A.J., 2002. Significance of mud volcanism. Rev. Geophys. 40 (2), 1005.
Lamb, M.P., et al., 2006. Can springs cut canyons into rock. J. Geophys. Res. 111, E07002. doi:10.1029/2005JE002663.
Lamb, M.P., et al., 2007. Formation of amphitheater-headed valleys by waterfall erosion after large-scale slumping on Hawai'I. Geol. Soc. Am. Bull. 209, 805–822.
Lamb, M.P., et al., 2008. Formation of Box Canyon, Idaho, by magaflood: implications for seepage erosion on Earth and Mars. Science 320, 1067–1070.
Lanagan, P.D., McEwen, A.S., Keszthelyi, L.P., Thordarson, T., 2001. Rootless cones on Mars indicating the presence of shallow equatorial ground ice in recent times. Geophys. Res. Lett. 28, 2365–2368.
Lane, M.D., Christensen, P.R., 2000. Convection in a catastrophic flood deposit as the mechanism for the giant polygons on Mars. J. Geophys. Res. 105 17,617–17,628.
Lapotre, M.G., Lamb, M.P., Williams, R.M.E., 2016. Canyon formation constraints on the discharge of catastrophic outburst floods of Earth and Mars. J. Geophys. Res. 121, 1232–1263. doi:10.1002/2016JE005061.
Laskar, J., Correia, A.C.M., Gastineau, M., Joutel, F., Levrard, B., Robutel, P., 2004. Long term evolution and chaotic diffusion of the insolation quantities of Mars. Icarus 170, 343–364.
Lopes, R.M.C., Kirk, R.L., Mitchell, K.L., LeGall, A., Barnes, J.W., Hayes, A., Kargel, J., Wye, L., Radebaugh, J., Stofan, E.R., Janssen, M., Neish, C., Wall, S., Wood, C.A., Lunine, J.I., Malaska, M., 2013. Cryovolcanism on Titan: new results from Cassini RADAR and VIMS. J. Geophys. Res. Planets 118, 1–20. doi:10.1002/jgre.20062.
Lorenz, V., 1973. On the formation of maars. Bull. Volcanol. 37, 183–204.
Lorenz, V., 1986. On the growth of maars and diatremes and its relevance to the formation of tuff rings. Bull. Volcanol. 48, 265–274.
Mahaney, W.C., et al., 2004. Ancient wet Aeolian environments on Earth: clues to presence of fossil/live microorganisms on Mars. Icarus 171, 39–53.
Malin, M.C., Carr, M.H., 1999. Ground-water formation of Martian Valleys. Nature 397, 589–591.
Malin, M.C., Bell III, J.F., Cantor, B.A., Caplinger, M.A., Calvin, W.M., Clancy, R.T., Edgett, K.S., Edwards, L., Haberle, R.M., James, P.B., Lee, S.W., Ravine1, M.A., Thomas, P.C., Wolff, M.J., 2007. ConTeXt Camera investigation on board the Mars Reconnaissance Orbiter. J. Geophys. Res. 112, E05S04. doi:10.1029/2006JE002808.
Mazzini, A., 2009. Mud volcanism: processes and Implications. Mar. Petrol. Geol. 26, 1677–1896.
McEwen, A.S., Malin, M.C., Carr, M.H., Hartmann, W.K., 1999. Voluminous volcanism on early Mars revealed in Valles Marineris. Nature 397, 584–586.
McEwen, A.S., et al., 2007. Mars Reconnaissance Orbiter's High Resolution Imaging Science Experiment (HiRISE). J. Geophys. Res. 112, E05S02. doi:10.1029/2005/JE002605.
McGowan, E.M., 2009. Spatial distribution of putative water related features in Southern Acidalia/Cydonia Mensae, Mars. Icarus 202, 78–89.
McGowan, E.M., 2011. The Utopia/Isidis overlap: possible conduit for mud volcanism on Mars. Icarus 212, 622–628.
McGill, G.E., 1986. The giant polygons of Utopia, Northern Martian plains. Geophys. Res. Lett. 13, 705–708.
Mège, D., Masson, P., 1996. A plume tectonics model for the Tharsis province, Mars. Planet. Space Sci. 44, 1499–1546.
Michael, G.G., Neukum, G., 2010. Planetary surface dating from crater size-frequency distribution measurements: partial resurfacing events and statistical age uncertainty. Earth Planet. Sci. Lett. 294, 223–229.
Mollel, G.F., Swisher III, C.C., Feigenson, M.D., Carr, M.J., 2008. Geochemical evolution of Ngorongoro Caldera, Northern Tanzania: implications for crust–magma interaction. Earth Planet. Sci. Lett. 271, 337–347.
Moore, J.M., 1990. Nature of the mantling deposit in the heavily cratered terrain ofnortheastern Arabia, Mars. J. Geophys. Res. 95, 14279–14289. doi:10.1029/JB095iB09p14279.
Moscardelli, L., Dooley, T., Dunlap, D., Jackson, M., Wood, L., 2012. Deep-water polygonal fault systems as terrestrial analogs for large-scale Martian polygonal terrains. GSA Today 22, 4–9.
Murchie, S., et al., 2007. Compact reconnaissance imaging spectrometer for Mars (CRISM) on Mars reconnaissance orbiter (MRO). J. Geophys. Res. 112, E05S03. doi:10.1029/2006JE002682.
Murchie, S.L., et al., 2009. Compact reconnaissance imaging spectrometer for Mars investigation and data set from the Mars Reconnaissance Orbiter's primary science phase. J. Geophys. Res. 114, E00D07. doi:10.1029/2009JE003344.
Mustard, J.F., Cooper, C.D., Rifkin, M.K., 2001. Evidence for recent climate change on Mars from the identification of youthful near-surface ground ice. Nature 412, 411–414.
Niemann, H., Lösekann, T., de Beer, D., Elvert, M., Nadalig, T., Knittel, K., Amann, R., Sauter, E.J., Schlüter, M., Klages, M., Foucher, J.-P., Boetius, A., 2006. Novel microbial communities of the Haakon Mosby mud volcano and their role as a methane sink. Nature 443, 854–858.
Noguchi, R., Kurita, K., 2015. Unique characteristics of cones in Central Elysium Planitia, Mars. Planet. Space Sci. 111, 44–54.
Ody, A., Poulet, F., Bibring, J.P., Loizeau, D., Carter, J., Gondet, B., Langevin, Y., 2013. Global investigation of olivine on Mars: insights into crust and mantle compositions. J. Geophys. Res. 118, 234–262.
Oehler, D.Z., Allen, C.C., 2010. Evidence for pervasive mud volcanism in Acidalia Planitia, Mars. Icarus 208, 636–657.
Oehler, D.Z., Allen, C.C., 2012. Giant polygons and mounds in the lowlands of Mars: signatures of an ancient ocean. Astrobiology 12, 601–615.
Oehler, D.Z., 2014. Giant polygons (Mars). In: Harditai, Kereszturi (Eds.), Encyclopedia of Planetary Landforms. Springer Science+Business Media, New York doi:10.1007/978-1-4614-9213-9_173-1.
Okubo, C.H., 2016. Morphologic evidence of subsurface sediment mobilization and mud volcanism in Candor and Coprates Chasmata, Valles Marineris, Mars. Icarus 269, 23–37.
Panter, K.S., McIntosh, W.C., Smellie, J.L., 1994. Volcanic history of Mount Sidley, a major alkaline volcano in Mrie Byrd Land, Antarctica. Bull. Volcanol. 56, 361–376.
Parker, T.J., Gorsline, D.S., 1991. Where is the source for Uzboi Vallis, Mars? In: *Lunar Planet Sci.* XXII, pp. 1033–1034.
Pechmann, J.C., 1980. The origin of polygonal troughs on the northern plains of Mars. Icarus 42, 185–210.
Pelkey, S.M., et al., 2007. CRISM multispectral summary products: parameterizing mineral diversity on Mars from reflectance. J. Geophys. Res. 112, E08S14. doi:10.1029/2006JE002831.
Pieri, D.C., 1980. Martian valleys: morphology, distribution, age, and origin. Science 210, 895–897.
Plescia, J.B., 1994. Geology of the small Tharsis volcanoes: Jovis Tholus, Ulysses Patera, Biblis Patera, Mars. Icarus 111, 246–269.
Pondrelli, M., et al., 2011. Mud volcanoes in the geologic record of Mars: the case of Firsoff crater. Earth Planet. Sci. Lett. 304, 511–519.
Robbins, S.J., Di Achille, G., Hynek, B.M., 2011. The volcanic history of Mars: high-resolution crater-based studies of the calderas of 20 volcanoes. Icarus 211, 1179–1203.
Robbins, S.J., Hynek, B.M., Lillis, R.J., Bottke, W.F., 2013. Large impact crater histories of Mars: the effect of different model crater age techniques. Icarus 225, 173–184. doi:10.1016/j.icarus.2013.03.019.
Russell, W.J., Brisbin, W.C., 1990. Primary fractures within a tuff cone, North Menan Butte, Idaho, U.S.A.. J. Volcanol. Geotherm. Res. 40, 11–22.
Sautter, V., Toplis, M.J., Wiens, R.C., Cousin, A., Fabre, C., Gasnault, O., Maurice, S., Forni, O., Lasue, J., Ollila, A., Bridges, J.C., Mangold, N., Le Mouélic, S., Fisk, M., Meslin, P.-Y., Beck, P., Pinet, P., Le Deit, L., Rapin, W., Stolper, E.M., Newsom, H., Dyar, D., Lanza, N., Vaniman, D., Clegg, S., Wray, J.J., 2015. In Situ evidence for continental crust on early Mars. Nature Geosci. 8, 605–609.
Schulze-Makuch, D., Dohm, J.M., Fan, C., Fairén, A.G., Rodrigues, J.A.P., Baker, V.R.., Fink, W., 2007. Exploration of hydrothermal targets on Mars. Icarus 189, 308–324.
Schulze-Makuch, D., Haque, S., Antonio, M.R.S., Ali, D., Hosein, R., Song, Y.C., Yang, J., Zaikova, E., Beckles, D.M., Guinan, E., Lehto, H.J., Hallam, S.J., 2011. Microbial life in a liquid asphalt desert. Astrobiology 11, 241–258.
Scott, D.H., Tanaka, K.L., (1986) Geological map of the western equatorial region of Mars. *US Geological Survey* I-1802-A.
Scott, D.H., Dohm, J.M., 1990. Faults and ridges: historical development in Tempe Terra and Ulysses Patera regions of Mars. In: Lunar and Planetary Science Conference, 20th, Houston, March 13-17, 1989, Proceedings. Houston. Lunar and Planetary Institute, pp. 503–513.
Self, S., Kienle, J., Huot, J.-P., 1980. Ukinrek Maars, Alaska, II. Depostis and formation of the 1977 craters. J. Volcano. Geotherm. Res. 7, 39–65.
Shedidan, M.F., Wohletz, K.H., 1983. Hydrovolcanism: basic considerations and review. J. Volcanol. Geotherm. Res. 17, 1–29.
Skidmore, M.L., Foght, J.M., Sharp, M.J., 2000. Microbial Life beneath a high arctic glacier. Appl. Environ. Microbiol. 66, 3214–3220.
Skinner Jr., J.A., Mazzini, A., 2009. Martian mud volcanism: Terrestrial analogs and implications for formational scenarios. Mar. Petrol. Geol.. http://dx.doi.org/10.1016/j.marpetgeo.2009.02.006.
Slater, J.A., Garvey, G., Johnston, C., Haase, J., Heady, B., Kroenung, G., Little, J., 2006. The SRTM data 'finishing' process and products. Photogramm. Eng. Remote Sens. 72, 237–247.

Smith, D.E., Zuber, M.T., Frey, H.V., Garvin, J.B., Head, J.W., Muhleman, D.O., Pettengill, G.H., Phillips, R.J., Solomon, S.C., Zwally, H.J., Banerdt, W.B., Duxbury, T.C., Golombek, M.P., Lemoine, F.G., Neumann, G.A., Rowlands, D.D., Aharonson, O., Ford, P.G., Ivanov, A.B., Johnson, C.L., McGovern, P.J., Abshire, J.B., Afzal, R.S., Sun, X., 2001. Mars Orbiter Laser Altimeter: experiment summary after the first year of global mapping of Mars. J. Geophys. Res. 106, 23689–23722.

Smith, D., Neumann, G., Arvidson, R.E., Guinness, E.A., Slavney, S., 2003. Mars Global Surveyor Laser Altimeter Mission Experiment Gridded Data Record. NASA Planetary Data System MGS-M-MOLA-5-MEGDR-L3-V1.0.

Soare, R.J., Conway, S.J., Pearce, G., Dohm, J.M., Grindrod, P.M., 2013. Possible crater-based pingos, paleolakes and periglacial landscapes in the high latitudes of Utopia Planitia, Mars. Icarus 225, 971–981.

Soare, R.J., Conway, S.J., Dohm, J.M., El-Maarry, M.R., 2014a. Possible open-system (hydraulic) pingos in and around the Argyre impact region of Mars. Earth Planet. Sci. Lett. 398, 25–36.

Soare, R.J., Conway, S.J., Dohm, J.M., El-Maarry, M.R., 2014b. Possible ice-wedge polygons and recent landscape modification by "wet" periglacial processes in and around the Argyre impact basin, Mars. Icarus 233, 214–228.

Soare, R.J., Conway, S.J., Gallagher, C., Dohm, J.M., 2017. "Ice-rich" (periglacial) vs "icy" (glacial) depressions in the Argyre region, Mars: a proposed cold-climate dichotomy of landforms. Icarus 282, 70–83. doi:10.1016/j.icarus.2016.09.009.

Souness, C., Hubbard, B., Milliken, R.E., Quincey, D., 2012. An inventory and population-scale analysis of martian glacier-like forms. Icarus 217, 243–255.

Tanaka, K.L., 1997. Sedimentary history and mass flow structures of Chryse and Acidalia Planitiae, Mars. J. Geophys. Res. 102, 4131–4150.

Tanaka, K.L., 2000. Dust and ice deposition in the martian geologic record. Icarus 144, 254–266.

Tanaka, K.L., J.A. Skinner, Jr., J.M. Dohm, R.P. Irwin III, E.J. Kolb, C.M. Fortezzo, T. Platz, G.G. Michael, and T.M. Hare (2014) Geologic map of Mars, *U.S. Geological Survey Scientific Investigations Map 3292*.

Thordarson, T., Höskuldsson, Á., 2008. Postglacial volcanism in Iceland. Jökull 58, 197–228.

Thorarinsson, S., 1953. The crater groups in Iceland. Bull. Volcanol. 14, 3–44.

Viviano-Beck, C.E., et al., 2014. Revised CRISM spectral parameters and summary products based on the currently detected mineral diversity on Mars. J. Geophys. Res. 119, 1403–1431.

Williams, D.A., et al., 2007. Hadiaca Patera: insights into its volcanic history from Mars Express High Resolution Stereo Camera. J. Geophys. Res. 112, E10004. doi:10.1029/2007JE002924.

Williams, J.-P., Paige, D.A., Manning, C.E., 2003. Layering in the wall rock of Valles Marineris: intrusive and extrusive magmatism. Geophys. Res. Lett. 30, 1623. doi:10.1029/2003GL017662.

Williams, J.-P., et al., 2014. A large vent structure within Argyre basin. Mars, *Lunar Planet. Sci. Conf.*, 45th Abstract 2807.

Williams, J.-P., 2016. Volcanism and giant polygons within Argyre basin. Mars, *Lunar Planet. Sci. Conf.*, 47th Abstract 2423.

Wilson, L., Head, J.W., 2002. Heat transfer and melting in subglacial basaltic volcanic eruptions: implications for volcanic deposit morphology and meltwater volumes. In: Smellie, J.L., Chapman, M.G. (Eds.), *Volcano-ice Interaction On Earth and Mars*. Geological Society, London, pp. 5–26. (Special publications 202).

Wray, J.J., Hansen, S.T., Dufek, J., Swayze, G.A., Murchie, S.L., Seelos, F.P., Skok, J.R., Irwin III, R.P., Ghiorso, M.S., 2013. Prolonged magmatic activity on Mars inferred from the detection of felsic rocks. Nature Geosci 6, 1013–1017.

Wyrick, D., et al., 2004. Distribution, morphology, and origins of martian pit crater chains. J. Geophys. Res. 109, E06005. doi:10.1029/2004JE002240.

Yakimov, M.M., Giuliano, L., Crisafi, E., Chernikova, T.N., Timmis, K.N., Golyshin, P.N., 2002. Microbial community of a saline mud volcano at San Biagio-Belpasso, Mt. Etna (Italy). Appl. Environ. Microbio. 4, 249–256.

Zuber, M.T., Smith, D.E., Solomon, S.C., Muhleman, D.O., Head, J.W., Garvin, J.B., Abshire, J.B., Bufton, J.L., 1992. The Mars Observer Laser Altimeter investigation. J. Geophys. Res. 97, 7781–7797.